UCLA
Computational and Applied Mathematics

Finite Element Implementation at Finite Strain and Assessment of a Prediction Model for Crack Growth in Strain Hardening Porous Ductile Materials

Koffi Enakoutsa
Yuelian Li

Department of Mathematics
University of California, Los Angeles
Los Angeles, CA, 90095-1555

Contents

List of Figures

List of Tables

1. Abstract

Accurately predicting crack extension is imperative for maintaining structural integrity in metal structures subjected to diverse loads. The Gurson model and its extensions are widely accepted for describing ductile fracture stages, particularly in porous materials with a rigid-perfectly plastic matrix. However, Gurson's approach of summarizing strain-hardening behavior into a single parameter proves limiting when considering a strain-hardening matrix. Perrin proposed a model addressing these limitations by incorporating two types of strain hardening parameters derived from an approximate analysis of a strain-hardening hollow sphere under axisymmetric loading. This paper aims to present a numerical implementation and assessment of Perrin's model in predicting ductile fracture under large deformations, considering isotropic, kinematics, and mixed isotropic-kinematics hardening scenarios. The effectiveness of the model is demonstrated by comparing numerical simulations of fracture with experimental observations in pre-cracked specimens. Given the challenges in achieving global elastic-plastic convergence for these large-scale simulations, an approach involving stiffness tangent moduli was employed to maintain quadratic convergence in global Newton method iterations.

2. Introduction

The integrity of engineering metal structures subjected to dynamic, cyclic, or quasi-static loads necessitates a comprehensive investigation of crack initiation and propagation. However, the primary challenge lies in finding a predictive tool capable of not only identifying crack initiation but also accurately predicting the subsequent crack extension. In the realm of ductile fracture, which stands as the predominant failure mode in metals under both room and high-temperature conditions, the micro-mechanically based model proposed by Gurson [12], along with its heuristic extensions by Tvergaard [22] and Tvergaard and Needleman [23], has gained widespread acceptance for describing the three successive stages of ductile fracture: cavity nucleation, growth, and coalescence.

Numerous studies have demonstrated the effectiveness of the Gurson model in characterizing crack propagation in pre-cracked metal structures, as well as in small uncracked laboratory test samples like smooth and notched round tensile specimens or plane strain specimens. Notably, the works of [23, 11, 2] have provided compelling evidence of the Gurson model's efficacy in accurately predicting the phenomenon known as "cup-cone" fracture in smooth axisymmetric tensile specimens. This phenomenon is characterized by the initial radial propagation of the crack from the axis, followed by a subsequent deviation at approximately a 45 $^\circ$ angle from the plane when it nears the cylindrical free surface.

An extension of the Gurson model [12] developed some years ago by Perrin and Leblond [13], presents a certain number of theoretical improvements compared to the model "R/R_0" and Rousselier's damage model [21]:

- better consideration of the interactions between growth of cavities and hardening, and introduction of the possibility of kinematic or mixed isotropic $\Big/$kinematic hardening;
- better modeling of coalescence;
- taking into account the nucleation, brutal or continuous, of the cavities, which can allow for the simulation of the behavior of specimens in stainless steel aged by irradiation for instance;
- incorporation of damage delocalization into the model itself, not just through the imposition of a minimum mesh size. This makes it possible to overcome the usual restrictions on the shape and size of the meshes.

In addition, the experience has revealed other advantages of the Perrin's model and/or its numerical implementation, of a more computational nature:

- The model accommodates square meshes, unlike that of Rousselier's damage model [21], which required the use of elongated rectangular meshes forcing the crack to remain in its plane. This made it possible to simulate the "cup-cone fracture" experiment, in which the crack deviates at 45° from its initial path[1].
- The model adequately reproduces the behavior of homothetic test specimens of small dimensions, a result which could not be obtained until now. The precise origin of this improvement, however, is unclear.

[1] The coalescence, neglected in the model of Rousselier's damage model [21], is only taken into account in a relatively coarse way in the model "R/R_0", because of the absence of coupling plasticity damage.

In the realm of crack propagation, it is common for the process to occur in areas of the materials where strain and damage concentrate. These localized regions exhibit incredibly steep stress and damage gradients, leading to a significant reliance on the mesh size used in finite element (FE) computations. As the mesh size becomes finer, a peculiar phenomenon arises: damage and strain tend to concentrate within zero-width bands. This intricate issue is widely acknowledged when attempting to model the response of ductile materials. The challenge arises from the need for more precise data regarding both deformation and stress states in the post-localization regime of these materials.

A proposal to circumvent this drawback was presented by the authors and co-workers [4, 6, 7]. Their proposal consists of adding, following an earlier suggestion by Pijaudier-Cabot and Bazant [14], a characteristic length scale to the constitutive model. This addition is accomplished through the convolution of the damage evolution equation with a carefully chosen weight function. Referred to as the "damage delocalization technique," this approach has effectively eradicated the detrimental influence of mesh size variations in finite element computations related to problems associated with ductile fracture. This accomplishment has been acknowledged by many researchers such as Leblond *et al.* [15], Tvergaard and Needleman [24, 25], Enakoutsa [6], and Enakoutsa *et al.* [4].

Leblond *et al.* [15] proposed a heuristic approach, which unfortunately lacked a solid theoretical foundation. This limitation prompted Gologanu *et al.* [26] to develop a more comprehensive and physically-based alternative. In their work, Gologanu and colleagues derived an enhanced version of Gurson's model, known as the GLPD model, by refining the original homogenization procedure based on the classical conditions of homogeneous boundary strain rate outlined by Mandel [27] and Hill [18]. Gologanu *et al.* [26] introduced a quadratic relationship between the boundary velocity and the coordinates, aiming to account for the potential rapid variations of macroscopic strain rate encountered during strain localization over short distances comparable to the size of the elementary cell under consideration. The outcome of their homogenization procedure yielded a "micromorphic" model featuring the second gradient of the macroscopic velocity, generalized macroscopic stresses of "moment" type (a product of stress and distance), and a "micro-structural distance" associated with the average spacing between adjacent voids.

The Gurson plasticity criterion is commonly regarded as capable of describing the yield strength of a porous material (containing spherical-shaped voids) with a rigid-perfectly plastic matrix that follows the Von Mises yield criterion. In the case of a strain-hardening matrix, Gurson [12] suggests summarizing the true strain-hardening behavior into a single parameter. This involves replacing the highly heterogeneous true strain-hardening, observed at the microscopic scale, with an "equivalent" homogeneous strain-hardening behavior. This approach has some flaws. Indeed, the classical, precise solution to the hydrostatic loading problem of a hollow rigid-hardenable sphere was not compatible with the phenomenological model. Additionally, the previous prediction that the porosity curve, which represents the relationship between porosity and equivalent strain for a fixed triaxiality during any loading path, solely depended on the initial porosity and triaxiality, but not on the hardening exponent, was found to be incorrect. To address these challenges, Perrin [13] proposed a new model, which tackles the issues by utilizing an approximate analysis of a hollow rigid-hardenable sphere subjected to axisymmetric loading. Two type of strain hardening parameters are introduced into the Gurson model [12]. These parameters are determined through an approximate solution to the problem of an axisymmetrically deformed strain-hardening hollow sphere.

The objective of this paper is to discuss the numerical implementation and evaluation of the hardening

model proposed by Perrin [13]. For the numerical implementation, we shall consider three different cases: isotropic hardening, kinematic hardening, and mixed isotropic-kinematic hardening. For each case, we will address the ”problem of projection,” which involves adjusting the elastically computed stress tensor to align with the yield locus (plastic correction of the elastic predictor). It is worth noting that the isotropic hardening case has been previously discussed by Enakoutsa [6] and Enakoutsa *et al.* [4]. Therefore, only a few elements of the projection problem will be presented in this context. We account for large deformation by using the the Green-Naghdi derivative for the rates of the stress and the kinematics hardening tensor. We provide the numerical implementation of this derivative in the context of our finite element modeling. Also, because global elasto-plastic iterations might face convergence difficulties, stiffness tangent moduli are derived for maintaining quadratic convergence in global Newton iterations. The assessment of the model will consist of comparing the experimental and numerical results for typical ductile fracture tests.

The paper is organized as follows:

- Section 3 provides a brief description of the theoretical equations of Perrin model [13] including the isotropic, kinematics, and the mixed isotropic-kinematics hardening.
- Next, Section 4 discusses the numerical implementation of the model. The correction of the stress in “the projection problem ” for the three types of hardening are discussed.
- Next, Section 5 presents the numerical integration strategy for the case of large deformations and rotations where the deformation of a structure is significant and cannot be accurately approximated using small displacement theory.
- Finally, in Section 6, the results of some numerical simulations comparing the fracture of a typical axisymmetric pre-cracked specimen to experimental observations reported by Rousselier and Mudry [19] are discussed. Given the challenges in achieving global elastic-plastic convergence for these large-scale simulations, an approach involving stiffness tangent moduli was employed. The objective of this approach is to maintain quadratic convergence in global Newton iterations.

3. Theoretical equations of the model

The model is written in large deformations, in Eulerian formulation, the deformation rate $\mathbf{d}$ is supposed to admit the usual additive decomposition:

$$\mathbf{d} = \mathbf{d}^{\mathrm{e}} + \mathbf{d}^{\mathrm{p}} \tag{1}$$

The model equations include the expression of the elastic strain rate $\mathbf{d}^{\mathrm{e}}$, that of the plastic strain rate $\mathbf{d}^{\mathrm{p}}$ (plasticity criterion and associated flow rule); and the expressions for the evolution equations for the internal parameters (porosity and hardening parameters).

3.1. Elastic Strain Rate

The law of elasticity used is in fact (as usual in elasto-plasticity large deformations) a law of hypo-elasticity or weak elasticity (linear relation between the rate of stress and the rate of elastic deformation; it is written, at constant temperature :

$$\hat{\mathbf{\Sigma}} = \lambda\,(\mathrm{tr}\mathbf{d}^{\mathrm{e}})\,1 + 2\mu\mathbf{d}^{\mathrm{e}} \tag{2}$$

where λ and μ denote the Lamé coefficients and σ an objective derivative of the stress tensor $\propto$. In practice, two derivatives are used: that of Jaumann, defined by:

$$\hat{\mathbf{\Sigma}} = \dot{\mathbf{\Sigma}} + \mathbf{\Sigma}\cdot\mathbf{\Omega} - \mathbf{\Omega}\cdot\mathbf{\Sigma} \tag{3}$$

where $\mathbf{\Omega} = \frac{1}{2}\left(\nabla_{\mathbf{x}}\mathbf{U} - {}^{t}\nabla_{\mathbf{x}}\mathbf{U}\right)$ ($\mathbf{x}$ current position vector, $\mathbf{U}$ velocity vector) denote the rate of rotation, and that of Green-Naghdi, defined by the same formula Eq.(3) , but $\mathbf{\Omega}$ then being equal to $\mathbf{R}.\mathbf{R}^{-1}$ where $\mathbf{R}$ is the rotation involved in the polar decomposition of the the deformation gradient.

It should be noted that this model does not incorporate a damage-elasticity coupling (λ and μ do not depend on the porosity and are therefore constant if the temperature is), much less important in practice than the damage-plasticity coupling. In the case where the temperature θ varies, we add to the expression of σ a term proportional to $\dot{\theta}$:

$$\hat{\mathbf{\Sigma}} = \lambda\,(\mathrm{tr}\mathbf{d}^{\mathrm{e}})\,\mathbf{I} + 2\mu\mathbf{d}^{\mathrm{e}} + \frac{\mathrm{dE}}{\mathrm{Ed}\theta}\mathbf{\Sigma}\dot{\theta}. \tag{4}$$

where E denotes the Young's modulus. This formula implicitly assumes the temperature-independent Poisson's ratio. It is recalled that it ensures the cancellation of the stresses at high temperatures, and is reduced after integration with the traditional formula

$$\mathbf{\Sigma} = \lambda(\theta)\,(\mathrm{tr}\boldsymbol{\varepsilon}^{\mathrm{e}})\,\mathbf{I} + 2\mu(\theta)\boldsymbol{\varepsilon}^{\mathrm{e}} \tag{5}$$

in the case where small deformation assumptions are made.

3.2. Plastic Strain Rate

Let us first consider the case of an isotropic work hardening. The criterion of plasticity is written as:

$$\phi(\mathbf{\Sigma}) = \frac{\Sigma_{\mathrm{eq}}^2}{\Sigma_1^2} + 2p\, ch\left(\frac{3}{2}\frac{\Sigma_{\mathrm{m}}}{\Sigma_2}\right) - 1 - p^2 \leq 0. \tag{6}$$

In this expression, Σ_{eq} is the equivalent Von Mises stress ($= \left(\frac{3}{2}\mathrm{s_{ij}}\mathrm{s_{ij}}\right)^{\frac{1}{2}}$, $\mathbf{s}$ denoting the deviator of the stress), Σ_{m} the mean stress ($= (\frac{1}{3})\mathrm{tr}\,\Sigma$), Σ_1 and Σ_2 homogeneous quantities with constraints given in the expression will be specified later, p a parameter linked to the porosity f by the formula

$$p = \mathrm{q}f^*, \quad f^* = \begin{cases} f & \text{if } f \leq f_{\mathrm{c}} \\ f_{\mathrm{c}} + \gamma\,(f - f_{\mathrm{c}}) & \text{if } f > f_{\mathrm{c}} \end{cases} \tag{7}$$

where q is the Tvergaard parameter, f_{c} the critical porosity at the beginning of coalescence and γ the accelerating factor of cavity growth.

The flow rule associated by normality with this criterion is written:

$$\mathbf{d}^{\mathrm{p}} = \eta\frac{\partial\phi}{\partial\mathbf{\Sigma}} \tag{8}$$

where η denotes the plastic multiplier; by introducing the equivalent plastic strain rate:

$$\mathrm{d_{eq}} = \left(\frac{2}{3}\delta_{\mathrm{ij}}^{\mathrm{p}}\,\delta_{\mathrm{ij}}^{\mathrm{p}}\right)^{\frac{1}{2}} \tag{9}$$

where $\boldsymbol{\delta}^{\mathrm{P}}$ denotes the deviator of $\mathbf{d}^{\mathrm{P}}$, we can write this flow rule in the form of the expression:

$$\begin{cases} \boldsymbol{\delta}^{\mathrm{P}} = \dfrac{3}{2}\dfrac{\mathrm{d_{eq}}}{\Sigma_{\mathrm{eq}}}\mathbf{s} \\ \mathrm{d_m^p} = \dfrac{p}{2}\dfrac{\Sigma_1^2}{\Sigma_2\Sigma_{\mathrm{eq}}}\, sh\left(\dfrac{3}{2}\dfrac{\Sigma_{\mathrm{m}}}{\Sigma_2}\right)\mathrm{d_{eq}} \end{cases} \tag{10}$$

where $\mathrm{d_m^p} = \frac{1}{3}\ \mathrm{tr}\ \mathbf{d}^{\mathrm{P}}$ is the average part of the plastic strain rate. The evolution of the porosity is given by the following equation, which results from the approximate incompressibility (i.e., neglecting the elasticity) of the metallic matrix:

$$\dot{f} = 3(1 - f)\mathrm{d_m^p} \tag{11}$$

Finally, Σ_1 and Σ_2 are functions of the temperature θ and of two parameters of hardening noted ε_{eq} and ε_m [2] and defined by:

$$\varepsilon_{\mathrm{eq}} = \int_0^\tau \mathrm{d_{eq}}\ \mathrm{d}\tau, \quad \varepsilon_{\mathrm{m}} = \int_0^\tau \left|\mathrm{d_m^p}\right|\ \mathrm{d}\tau. \tag{12}$$

[2] The rather complicated expressions of Σ_1 and Σ_2 as a function of $\varepsilon_{\mathrm{eq}}$ and ε_{m} are given in Perrin [13]

Let us now consider the case of a kinematic hardening. The expression of the criterion of plasticity is:

$$\frac{\Sigma_{\rm eq}^2}{\Sigma_0^2} + 2p\ sh\left(\frac{3}{2}\frac{\Sigma_{\rm m}-\alpha_{\rm m}}{\Sigma_0}\right) - 1 - p^2 \leq 0 \tag{13}$$

where Σ_0 is the elastic limit (depending only on temperature) of the matrix, $\alpha_m = \frac{1}{3}$ tr α the mean part of the center α of the domain of elasticity and $\Sigma_{\rm eq}$ the equivalent von Mises stress defined here by

$$\Sigma_{\rm eq} = \left[\frac{3}{2}\left(s_{\rm ij}-a_{\rm ij}\right)\left(s_{\rm ij}-a_{\rm ij}\right)\right]^{\frac{1}{2}}, \tag{14}$$

$\mathbf{a}$ denoting the deviator of $\boldsymbol{\alpha}$. The expression of p is the same (Eq.(7) as for an isotropic hardening. The associated flow rule takes the form:

$$\begin{cases} \boldsymbol{\delta}^{\rm p} = \dfrac{3}{2}\dfrac{{\rm d}_{\rm eq}}{\Sigma_{\rm eq}}(\mathbf{s}-\mathbf{a}) \\ {\rm d}_{\rm m}^{\rm p} = \dfrac{p}{2}\dfrac{\Sigma_0}{\Sigma_{\rm eq}}\, sh\left(\dfrac{3}{2}\dfrac{\Sigma_{\rm m}-\alpha_{\rm m}}{\Sigma_0}\right){\rm d}_{\rm eq} \end{cases} \tag{15}$$

where $\delta^{\rm p}, {\rm d}_{\rm eq}$ and ${\rm d}_{\rm m}^{\rm p}$ are defined as before. The porosity evolution equation Eq.(11) is unchanged. Finally, the evolution of the center $\mathbf{a}$ of the domain of elasticity is given by:

$$\begin{cases} \hat{\mathbf{a}} = \dfrac{2}{3}\left(\dfrac{\partial\tilde{\alpha}_{\rm eq}}{\partial\varepsilon_{\rm eq}}\right)_T \boldsymbol{\delta}^{\rm p} + \dfrac{1}{\tilde{\alpha}_{\rm cq}}\left(\dfrac{\partial\tilde{\alpha}_{\rm eq}}{\partial\theta}\right)\mathbf{a}\dot{\theta} \\ \dot{\alpha}_{\rm m} = \left(\dfrac{\partial\tilde{\alpha}_{\rm m}}{\partial\varepsilon_{\rm m}}\right)_T {\rm d}_{\rm m}^{\rm p} + \dfrac{1}{\tilde{\alpha}_{\rm m}}\left(\dfrac{\partial\tilde{\alpha}_{\rm m}}{\partial\theta}\right)\alpha_{\rm m}\dot{\theta} \end{cases} \tag{16}$$

where $\hat{}$ denotes the same objective derivative as in Eq.(2) and Eq.(4) and where $\tilde{\alpha}_{\rm eq}$ and $\tilde{\alpha}_{\rm m}$ are functions [3] of the same hardening parameters $\varepsilon_{\rm eq}, \varepsilon_{\rm m}$ as previously. The partial derivatives $\left(\partial\tilde{\alpha}_{\rm eq}/\partial\varepsilon_{\rm eq}\right)$ and $(\partial\tilde{\alpha}_{\rm m}/\partial\varepsilon_{\rm m})$ are here taken at "triaxiality in deformation" T $= \varepsilon_{\rm m}/\varepsilon_{\rm eq}$ constant. The terms proportional to $\dot{\theta}$ ensure the cancellation of $\mathbf{a}$ and $\alpha_{\rm m}$, therefore of $\boldsymbol{\Sigma}$, at high temperatures. Let us consider finally the case of a mixed isotropic/kinematic hardening ρ indicating the proportion of kinematic hardening. The criterion is written:

$$\frac{\Sigma_{\rm eq}^2}{\left[\rho\Sigma_0+(1-\rho)\Sigma_1\right]^2} + 2p\ sh\left(\frac{3}{2}\frac{\Sigma_{\rm m}-\rho\alpha_{\rm m}}{\rho\Sigma_0+(1-\rho)\Sigma_2}\right) - 1 - p^2 \leq 0 \tag{17}$$

where

$$\Sigma_{\rm eq} = \left[\frac{3}{2}\left(s_{\rm ij}-\rho a_{\rm ij}\right)\left(s_{\rm ij}-\rho a_{\rm ij}\right)\right]^{\frac{1}{2}}, \tag{18}$$

and the flow rule

$$\begin{cases} \boldsymbol{\delta}^{\rm p} = \dfrac{3}{2}\dfrac{{\rm d}_{\rm eq}}{\Sigma_{\rm eq}}(\mathbf{s}-\rho\mathbf{a}) \\ {\rm d}_{\rm m}^{\rm p} = \dfrac{p}{2}\dfrac{\left[\rho\Sigma_0+(1-\rho)\Sigma_1\right]^2}{\left[\rho\Sigma_0+(1-\rho)\Sigma_2\right]\Sigma_{\rm eq}}\, sh\left(\dfrac{3}{2}\dfrac{\Sigma_{\rm m}-\rho\alpha_{\rm m}}{\rho\Sigma_0+(1-\rho)\Sigma_2}\right){\rm d}_{\rm eq}. \end{cases} \tag{19}$$

[3] the expressions of which are given in [13]

The laws of evolution of the porosity and of the hardening parameters are the same as previously.

In fact, the cavities being very generally generated by decohesion of the metal matrix around inclusions, f can not become lower than its initial value f_0 (if f is equal to f_0, the cavity is closed around inclusion and the latter prevents its volume from decreasing further). Consequently, all the previous equations are valid only if $f > f_0$, or else $f = f_0$ and $\dot{f} \geq 0 \Leftrightarrow sh \geq 0$ (sh representing the hyperbolic sine of :

$$\frac{3}{2}\frac{\Sigma_{\mathrm{m}}}{\Sigma_2}, \frac{3}{2}\frac{\Sigma_{\mathrm{m}} - \alpha_{\mathrm{m}}}{\Sigma_0} \text{ or } \frac{3}{2}\frac{\Sigma_{\mathrm{m}} - \rho\alpha_{\mathrm{m}}}{\rho\Sigma_0 + (1-\rho)\Sigma_2} \tag{20}$$

depending on the type of hardening). If $f = f_0$ and $sh < 0$, it is necessary to write that the behavior is that of a Von Mises material, which is in fact equivalent to setting $\mathrm{p} = 0$ in the previous equations.

3.3. Cavities' Nucleation

We have until now, for simplicity, implicitly ignored the phenomena of nucleation of the cavities. Let us now examine their impact. We distinguish two types of nucleation:

- sudden nucleation, governed by a stress criterion developed at the Ecole des Mines de Paris and whose expression is:

  $$\Sigma_1 + \alpha\left(\tilde{\Sigma}_{\mathrm{eq}} - \Sigma_0\right) \leq \Sigma_{\mathrm{c}} \tag{21}$$

  where Σ_1 denotes the greatest principal stress of the stress tensor Σ, α a dimensionless parameter, Σ_{c} a critical stress and $\tilde{\Sigma}_{\mathrm{eq}}$ the equivalent stress defined by:

  $$\tilde{\Sigma}_{\mathrm{eq}} = \left(\frac{3}{2}\, \mathrm{s}_{\mathrm{ij}}\mathrm{s}_{\mathrm{ij}}\right)^{\frac{1}{2}} \tag{22}$$

  ($\tilde{\Sigma}_{\mathrm{eq}}$ only coincides with Σ_{eq} in the case of isotropic hardening). As long as the inequality is strict in Eq. (90), the behavior is that of a Von Mises material ($\Leftrightarrow p = 0$); when the equality is achieved, f "jumps" abruptly to the value f_0 (and cannot then fall below this value again).

- Continuous nucleation. We distinguish in this case two contributions, denoted $\dot{f_{\mathrm{c}}}$ and $\dot{f_{\mathrm{g}}}$, in the growth rate f porosity. The first represents the rate of increase da at the growth of the cavities, and is given by formula Eq. (11). The second represents the rate of increase due to continuous germination, and is given by an empirical equation

  $$\dot{f_{\mathrm{g}}} = \mathrm{A}\dot{\mathrm{d}}_{\mathrm{eq}} \tag{23}$$

where A is a model parameter.

3.4. Damage Delocalization

For some applications (involving high stress and/or strain gradients), the porosity evolution equation is "delocalized". We then define local rates of increase of porosity by growth and germination $\dot{f}_{\mathrm{cl}}$ and $\dot{f}_{\mathrm{gl}}$, given

by formulas Eq.(11) and Eq.(23) respectively, and the true (non-local) growth rate is then given by the convolution formula:

$$\begin{aligned} f(\mathbf{x}) &= \frac{1}{\mathrm{C}(\mathbf{x})} \int_{\Omega} \dot{f}_{\mathrm{l}}(\mathbf{y}) \chi(\mathbf{x}-\mathbf{y}) \mathrm{d}\Omega_y \ , \\ \dot{f}_{\mathrm{l}}(\mathbf{y}) &\equiv \dot{f}_{\mathrm{cl}}(\mathbf{y}) + \dot{f}_{\mathrm{gl}}(\mathbf{y}) \ , \\ C(\mathbf{x}) &= \textstyle\int_{\Omega} \chi(\mathbf{x}-\mathbf{y}) \mathrm{d}\Omega_{\mathbf{y}} \ . \end{aligned} \tag{24}$$

Ω denotes here the studied domain and χ a weighting function, which we take Gaussian in practice:

$$\chi(\mathbf{z}) = exp\left(\frac{-|\mathbf{z}|^2}{l^2}\right), \tag{25}$$

$\mathbf{l}$ being a characteristic length (of the order of the spacing between cavities), which plays the same role as the minimum mesh size in the Rousselier model. Note that this delocalization study was thouroughly study by Enakoutsa *et al.* ([1], [4], [6], [7], [8], [9] , and [10])

4. Numerical Implementation

This section aims to present the digital implementation of the constitutive equations of the non-local Gurson model [12], as defined by Leblond *et al.* [15], for its integration into the finite element calculation code. The essential element of this numerical implementation is the necessary ”projection” operation onto the criterion. After specifying the time discretization of the problem, which establishes the notations used, and briefly recalling the two main steps (local and global) associated with the iterative solution of the problem, we describe the algorithm used for this projection.

4.1. Time Discretization

The constitutive equations of the models presented above are described by integro-differential relationships in time. Since direct integration of the continuous problem in time is very difficult, we adopt a step-by-step resolution method: we seek to determine the various mechanical parameters at time $t + \Delta t$ given these quantities at time t. Dealing with ductile materials (which exhibit dissipative behavior), we adopt an implicit Euler scheme for most variables. Different perspectives could be considered, but it is not customary because this scheme has become traditional for integrating the behavior relationships of dissipative materials. It is unconditionally stable and allows for exact verification of the coherence condition when the behavior is independent of time.

4.2. Overview of the Problem-Solving Approach

In general, solving a quasi-static evolution problem requires the coupled treatment of two sub-problems: ensuring structural equilibrium and incorporating behavior relations. The approach adopted in our finite calculations code favors displacements as unknowns (rather than internal variables). Roughly speaking, after time discretization, we are led to solve the following system: The equilibrium is expressed in terms of the principle of virtual powers:

$$\int_{\Omega} \mathbf{\Sigma} \cdot \varepsilon(\mathbf{v}) d\Omega = \int_{\Omega} f^d \cdot \mathbf{v} \, d\Omega + \int_{\partial\Omega} \mathbf{T}^d \cdot \mathbf{v} \, d \, \partial\Omega \qquad \forall \, \mathbf{v} \in V_0^{ad} \tag{26}$$

where V_0^{ad} represents the set of kinematically admissible fields, $\mathbf{\Sigma}$ is the unknown stress field, $\mathbf{T}^d$ and $\mathbf{f}^d$ are

the imposed volumetric and surface forces. The integration of the behavior relations provides the stress $\boldsymbol{\Sigma}$ at each point as a function of the displacement increment $\Delta\mathbf{u}$ through a nonlinear relationship. The equilibrium equation Eq. (26) is then written in the form:

$$\mathbf{R}(\Delta\mathbf{u}) = \mathbf{F}_i - \mathbf{F}_e = \mathbf{0}. \tag{27}$$

in the case of discretization using the finite element method. In equation Eq.(27), $\mathbf{R}$ is the vector of nodal residuals expressed as the difference between the internal nodal forces $\mathbf{F}_i$ and the external nodal forces $\mathbf{F}_e$. Since the system Eq.(27) is nonlinear, its solution cannot be directly obtained as in elasticity problems. The solution is obtained using an iterative method like Newton's method (or one of its variants), with iterations ending when equilibrium is considered achieved. Each iteration consists of two steps: a global step and a local step.

The **global step** consists of calculating the displacements at the structure's nodes, as well as the total strains and stresses at the Gauss points, assuming the plastic deformation increment $\Delta\boldsymbol{\Sigma}^{\mathrm{p}}$ between times t and $t + \Delta t$ is known at every point. In practice, during the first iteration, this increment is assumed to be zero (purely elastic calculation), and in subsequent iterations, it takes the value found at the end of the previous iteration. This step uses the equilibrium equations, the elastic behavior law, and the boundary conditions, resulting in solving a linear system over the entire structure. However, the plasticity equations are not used during this step.

The approach is analogous to solving a classical elasticity problem using the finite element method, with the difference that the total strain includes an additional contribution from plasticity, which plays the role of "initial deformation" (analogous to thermal deformation, for example).

During the **local step**, the final total deformation (or its increment $\Delta\varepsilon$), resulting from the previous global step, is considered as given at each point. Then, the increments of elastic and plastic deformation, $\Delta\varepsilon^{\mathrm{e}}$ and $\Delta\varepsilon^{\mathrm{p}}$, as well as the stress $\boldsymbol{\Sigma}$, are calculated using the equations of plasticity. In no way, during this step, will equilibrium equations or boundary conditions be used, which excludes solving a linear system over the entire structure. The solution algorithm is performed independently at different points.

The following diagram summarizes the different steps of the method.

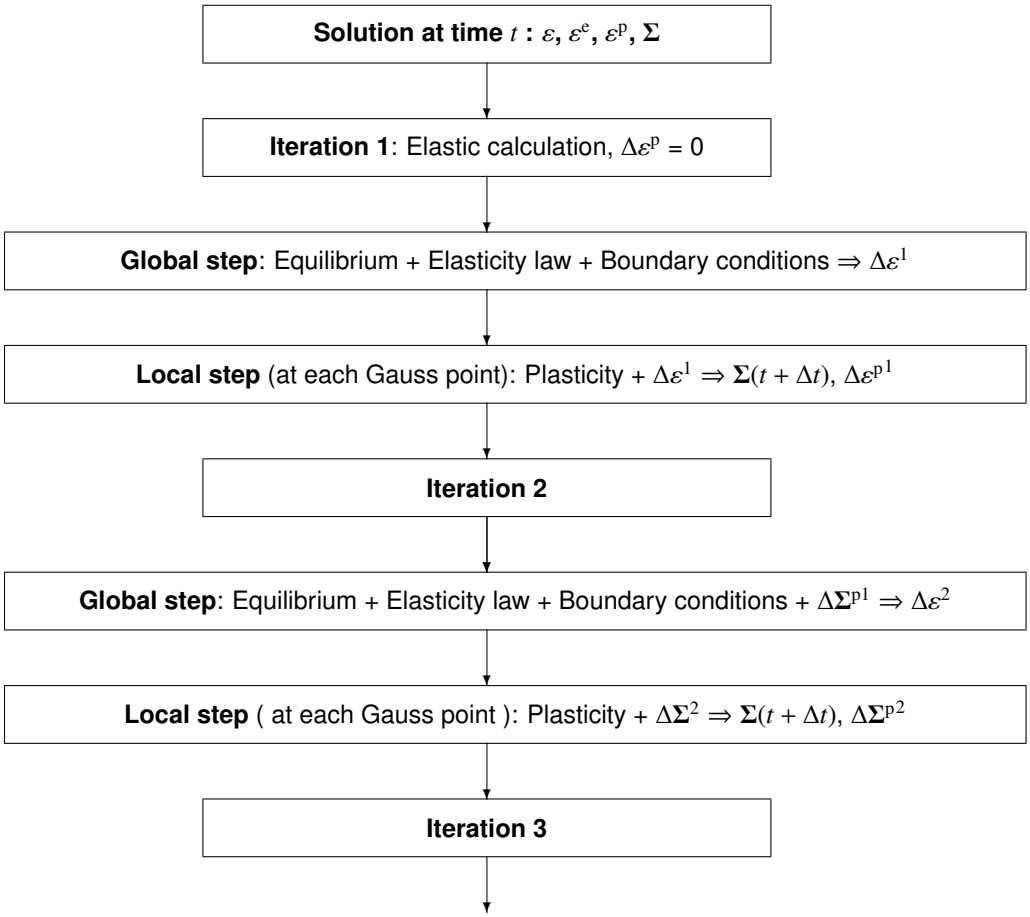

It should be noted that despite the somewhat complex nature that the programming of the global step may take, there is no need to worry about it when digitally implementing a new plasticity model into a finite element calculation code. The only developments required are related to the local step, which we will now focus on. The reason is quite simple: the model to be implemented is independent of this programming (in fact, it is a general routine that can be used by any other plasticity model). For this reason, we will only focus on the local step in the implementation of the ductile fracture model described above. We will only consider the points in the structure where we are looking for increments in plastic and elastic deformations and stresses. In practice, all Gauss points in the structure are processed successively, but again, there is no need to worry as an automatic procedure, valid for any model that we want to implement, takes care of it and is written once and for all.

Compared to the numerical implementation of the classical elasto-plasticity equations in large transformations, that of the ductile rupture models presents certain differences which mainly concern the so-called operation of “plastic stress correction” (calculation of the stresses and various other mechanical parameters at time $t + \Delta t$, knowing these quantities at time t as well as the increment $\Delta\varepsilon \equiv \mathbf{d}\Delta t$ of total deformation between these two times).

4.3. Implicit algorithm for projecting onto the criterion.

4.3.1. Generalities

The numerization of the constitutive equations of the Gurson model, whether in its local or non-local version, presents certain differences compared to the digitization of the classical von Mises elasto-plasticity equations. These differences mainly concern the "projection onto the criterion" or "plastic stress correction" operation, which involves calculating stresses and various other mechanical parameters at time $t + \Delta t$, given these quantities at time t as well as the total strain increment $\Delta\mathbf{v} \equiv \varepsilon\Delta t$ between these two instants. (Note that in large transformations, $\varepsilon\Delta t$ is not the variation of the linearized strain tensor, which is not defined. The notation $\Delta\mathbf{v}$ is used to simplify the expressions.)

In everything that follows, we will focus on the incremental problem defined between times t and $t + \Delta t$. Initially, we assume small strains to simplify the presentation. The quantities that appear will be considered at time $t + \Delta t$, unless they are marked with an upper index ^{0}, which indicates that they are considered at time t. The known quantities include $\mathbf{\Sigma}$ (stress), $\bar{\varepsilon}$ (strain), and $\Delta\varepsilon$ (the total strain increment between times t and $t + \Delta t$).

4.3.2. Correction of the Stress - Case of Isotropic Hardening

Let us write the discretized equations of the problem, denoting $\Delta\boldsymbol{\varepsilon} \equiv \mathbf{d}\Delta t$, $\Delta\boldsymbol{\varepsilon}^{\mathrm{e}} \equiv \mathbf{d}^{\mathrm{e}}\Delta t, \Delta\boldsymbol{\varepsilon}^{\mathrm{p}} \equiv \mathbf{d}^{\mathrm{p}}\Delta t, \Delta\mathbf{e}^{\mathrm{e}}$ and $\Delta\mathbf{e}^{\mathrm{p}}$ the deviatoric parts of $\Delta\boldsymbol{\varepsilon}^{\mathrm{e}}$ and $\Delta\boldsymbol{\varepsilon}^{\mathrm{p}}, \Delta\varepsilon^{\mathrm{e}}_{\mathrm{m}}$ and $\Delta\varepsilon^{\mathrm{p}}_{\mathrm{m}}$ their mean parts, assigning a ' the quantities taken at time $t + \Delta t$ (the non-primed quantities are taken at time t), and initially neglecting the effects due temperature variations and major transformations:

- Decomposition of the deformation increment:

$$\Delta\boldsymbol{\varepsilon} = \Delta\boldsymbol{\varepsilon}^{\mathrm{e}} + \Delta\boldsymbol{\varepsilon}^{\mathrm{p}} \tag{28}$$

- Elasticity law :

$$\Delta\mathbf{s} = 2\mu\Delta\mathbf{e}^{\mathrm{e}}, \tag{29}$$

$$\Delta\Sigma_{\mathrm{m}} = (3\lambda + 2\mu)\Delta\varepsilon^{\mathrm{e}}_{\mathrm{m}} \tag{30}$$

- Yield criteria :

$$\frac{{\Sigma'_{\mathrm{eq}}}^2}{\Sigma'^2_1} + 2\tilde{p}'\, ch\left(\frac{3}{2}\frac{\Sigma'_{\mathrm{m}}}{\Sigma'_2}\right) - 1 - \tilde{p}'^2 = 0 \tag{31}$$

- Plastic flow rule :

$$\Delta\mathbf{e}^{\mathrm{p}} = \frac{3}{2}\frac{\Delta\varepsilon_{\mathrm{eq}}}{\Sigma'_{\mathrm{eq}}}\mathbf{s}', \tag{32}$$

$$\Delta\varepsilon_{\mathrm{m}}^{\mathrm{p}} = \frac{\tilde{p}''}{2}\frac{\Sigma_1'^2}{\Sigma_2'\Sigma_{\mathrm{eq}}'} sh\left(\frac{3}{2}\frac{\Sigma_{\mathrm{m}}'}{\Sigma_2'}\right)\Delta\varepsilon_{\mathrm{eq}}. \tag{33}$$

- Definition of Σ_1' and Σ_2' :

$$\begin{array}{l}\Sigma_1' \equiv \Sigma_1\left(\varepsilon_{\mathrm{eq}}', \varepsilon_{\mathrm{m}}'\right), \\ \Sigma_2' \equiv \Sigma_2\left(\varepsilon_{\mathrm{eq}}', \varepsilon_{\mathrm{m}}'\right)\end{array} \tag{34}$$

- Evolution equation of the hardening parameters:

$$\begin{array}{l}\Delta\varepsilon_{\mathrm{eq}} = \left(\frac{2}{3}\Delta\mathrm{e}_{\mathrm{ij}}^{\mathrm{p}}\Delta\mathrm{e}_{\mathrm{ij}}^{\mathrm{p}}\right)^{\frac{1}{2}}. \\ \Delta\varepsilon_{\mathrm{m}} = \left|\Delta\varepsilon_{\mathrm{m}}^{\mathrm{p}}\right|.\end{array} \tag{35}$$

Only equations Eq.(31) and Eq.(33) call for specific comments here:

- To be perfectly logical, it would be necessary to use in Eq.(31), which constitutes the writing of the criterion at the instant $t + \Delta t$, the quantity $p' \equiv p(t + \Delta t)$ deriving, via Eq.(7), from the real porosity f' at this instant. This porosity being unknown, the algorithm is then implicit in relation to this variable (as in relation to the others). The numerical experiment however showed that the convergence is very difficult, even impossible, with such an algorithm, and that one can, in practice, obtain results only with an explicit algorithm compared to the porosity (but however implicit against all other parameters). We therefore replace in Eq.(31) the quantity p' by an approximation noted $\tilde{p}'$, deriving via Eq.(7), from the estimation of $\tilde{f}'$ of $f' \equiv f(t + \Delta t)$ given by

$$\tilde{f}' \equiv f(t) + \dot{f}(t)\Delta t. \tag{36}$$

  This of course requires storing the rate of increase $\dot{f}$ of the porosity.

- In equation (33), which gives the increase in average plastic deformation between the times t and $t + \Delta t$, the most precise would be to use the quantity $p'' = p(t + \Delta t/2)$ (deriving from the true porosity $(f''$ to $t + \Delta t/2)$ In order to preserve however the explicit character of the algorithm with respect to porosity, we replaces p'' by the approximation $\tilde{p}''$ derived from the approximate porosity

$$\tilde{f}'' \equiv f(t) + f(t)\frac{\Delta t}{2}. \tag{37}$$

The beginning of the resolution of these equations follows the classic approach: we add $\mathbf{s}$ to the two members of Eq.(29) taking into account Eq.(30) and Eq.(31) :

$$\mathbf{s}' \equiv \mathbf{s} + \Delta\mathbf{s} = \mathbf{s} + 2\mu\Delta\mathbf{e} - 2\mu\Delta\mathbf{e}^{\mathrm{p}} = \mathbf{s}^* - 3\mu\frac{\Delta\varepsilon_{\mathrm{eq}}}{\Sigma_{\mathrm{eq}}'}\mathbf{s}' \tag{38}$$

where

$$\mathbf{s}^* \equiv \mathbf{s} + 2\mu\Delta\mathbf{e} \quad (\Delta\mathbf{e} \equiv \text{ deviator of } \Delta\boldsymbol{\varepsilon}) \tag{39}$$

is the final stress deviator "computed elastically", i.e. assuming the increment $\Delta\varepsilon$ of purely elastic total deformation (known quantity since we know $\mathbf{s}$ and Δe). This implies that, as usual, $\mathbf{s}'$ and $\mathbf{s}^*$ are parallel, so that we can replace

$\mathbf{s}'\Big/\Sigma'_{\rm eq}$ by $\mathbf{s}^*\Big/\Sigma^*_{\rm eq}$ where $\left(\Sigma^*_{\rm eq} \equiv \left(\frac{3}{2}s^*{}_{\rm ij}s^*{}_{\rm ij}\right)^{\frac{1}{2}}\right)$ in the flow rule Eq.(33) and the calculation of Δep is reduced to that of $\Delta\varepsilon_{\rm eq}$. Moreover, taking the Von Mises function of the two members, we also deduce that

$$\Sigma^*_{\rm eq} - \Sigma'_{\rm eq} = 3\mu\Delta\varepsilon_{\rm eq} \tag{40}$$

again a classic equation. By adding in the same way $\Sigma_{\rm m}$ to the two members of Eq.(30) taking into account Eq.(29), we obtain the same

$$\Sigma^*_{\rm m} - \Sigma'_{\rm m} = (3\lambda + 2\mu)\Delta\varepsilon^{\rm p}_{\rm m}, \tag{41}$$

where

$$\Sigma^*_{\rm m} \equiv \Sigma_{\rm m} + (3\lambda + 2\mu)\Delta E_{\rm m} \tag{42}$$

($\Delta E_{\rm m}$ mean part of $\Delta\varepsilon$[4]) denotes the "elastically calculated" (known) final mean stress. Combining Eq. (29) and Eq. (42), we get:

$$\frac{\Delta\varepsilon^{\rm p}_{\rm m}}{\Delta\varepsilon_{\rm eq}} = \frac{3\mu}{3\lambda + 2\mu}\frac{\Sigma^*_{\rm m} - \Sigma'_{\rm m}}{\Sigma^*_{\rm eq} - \Sigma'_{\rm eq}}. \tag{43}$$

Relating this equation to Eq. (33), we get

$$\frac{3\mu}{3\lambda + 2\mu}\frac{\Sigma^*_{\rm m} - \Sigma'_{\rm m}}{\Sigma^*_{\rm eq} - \Sigma'_{\rm eq}} = \frac{\tilde{p}''}{2}\frac{\Sigma'^2_1}{\Sigma'_2\Sigma'_{\rm eq}}sh\left(\frac{3}{2}\frac{\Sigma'_{\rm m}}{\Sigma'_2}\right). \tag{44}$$

The problem is reduced to the resolution of equations Eq. (31), Eq. (34), Eq. $(35)_2$, Eq. (40), Eq. (41) and Eq. (44) with respect to the unknowns $\Sigma'_{\rm eq}, \Sigma'_{\rm m}, \Sigma'_1, \Sigma'_2, \Delta\varepsilon_{\rm eq}, \Delta\varepsilon^{\rm p}_{\rm m}$ and $\Delta\varepsilon_{\rm m}$. For this, we adopt an iterative approach with respect to the unknowns $\Delta\varepsilon_{\rm eq}, \Delta\varepsilon^{\rm p}_{\rm m}, \Delta\varepsilon_{\rm m}, \Sigma'_1, \Sigma'_2$: starting from certain initial values of these parameters, we solve (we will see how) Eq.(31) and Eq.(44) by compared to $\Sigma'_{\rm eq}$ and $\Sigma'_{\rm m}$, we deduce $\Delta\varepsilon_{\rm eq}, \Delta\varepsilon^{\rm p}_{\rm m}$ and $\Delta\varepsilon_{\rm m}$ with Eq. (40), Eq. (41) and Eq. $(35)_2$, then Σ'_1 and Σ'_2 by Eq. (34) and we iterate the process until convergence.

The whole problem therefore consists in simultaneously solving equations Eq. (31) and Eq. (44) with respect to $\Sigma'_{\rm eq}$ and $\Sigma'_{\rm m}$, the other parameters being assumed to be known. For this, we use the following parametrization (inspired by that of an ellipse) of the flow surface Eq. (31):

$$\begin{cases} \Sigma'_{\rm eq} = (1 - \tilde{p}')\,\Sigma'_1 cos\varphi \\ \Sigma'_{\rm m} = \frac{2}{3}\Sigma'_2 sgn(\varphi) Arg\ sh\left[1 + \frac{(1-\tilde{p}')^2}{2p'}sin^2\varphi\right]. \end{cases} \qquad \left(-\frac{\pi}{2} \le \varphi \le \frac{\pi}{2}\right). \tag{45}$$

[4]The notation $E_{\rm m}$ is used here to avoid confusion with the hardening parameter $\varepsilon_{\rm m}$.

The problem is then to solve the following equation, taken from Eq. (44), with respect to the unique variable φ:

$$\mathrm{F}(\varphi) = \mathrm{a}\left[\Sigma^*_{\mathrm{m}} - \Sigma'_{\mathrm{m}}(\varphi)\right] cos\varphi\, \tilde{p}''\left[\Sigma^*_{\mathrm{eq}} - \Sigma'_{\mathrm{eq}}(\varphi)\right] sh\left[\frac{3}{2}\frac{\Sigma'_{\mathrm{m}}(\varphi)]}{\Sigma'_2}\right] = 0 \tag{46}$$

where

$$\mathrm{a} \equiv 2\left(1-\tilde{p}'\right)\frac{\Sigma'_2}{\Sigma'_1}\frac{3\mu}{3\lambda+2\mu} \tag{47}$$

It is sufficient for that to use the method of Newton; one easily calculates for this purpose:

$$\begin{aligned} F(\varphi) = -\, sin\varphi \Bigg(& \mathrm{a}\left[\Sigma^*_{\mathrm{m}} - \Sigma'_{\mathrm{m}}(\varphi) + \frac{2\left(1-\tilde{p}'\right)^2\Sigma'_2\cos^2\varphi}{3\tilde{p}'\, sh\left(\frac{3}{2}\frac{\Sigma'_{\mathrm{m}}(\varphi)}{\Sigma'_2}\right)}\right] \\ & + \tilde{p}''\left(1-\tilde{p}'\right)\Sigma'_1 sh\left(\frac{3}{2}\frac{\Sigma'_{\mathrm{m}}(\varphi)}{\Sigma'_2}\right) \\ & + \frac{\tilde{p}''}{\tilde{p}'}\left(1-\tilde{p}'\right)^2\left[\Sigma^*_{\mathrm{eq}} - \Sigma'_{\mathrm{eq}}(\varphi)\right] cos\varphi\, coth\left(\frac{3}{2}\frac{\Sigma'_{\mathrm{m}}(\varphi)}{\Sigma'_2}\right)\Bigg). \end{aligned} \tag{48}$$

Most of the numerical solution therefore consists of two nested loops, the outer loop carrying out the iterations on the parameters $\Sigma'_1, \Sigma'_2, \Delta\varepsilon_{\mathrm{eq}}, \Delta\varepsilon^{\mathrm{p}}_{\mathrm{m}}$ and $\Delta\varepsilon_{\mathrm{m}}$, the inner loop solving Eq.(46) by the Newton's method. Once this calculation is complete, the program evaluates the local porosity increment Δf_1 using the following discretized version of equations Eq. (11) and Eq. (23):

$$\Delta f_1 = \Delta f_{\mathrm{lc}} + \Delta f_{\mathrm{lg}},\ \Delta f_{\mathrm{lc}} = 3\left(1-\tilde{f}'\right)\Delta\varepsilon^{\mathrm{p}}_{\mathrm{m}},\ \Delta f_{\mathrm{lg}} = \mathrm{A}\varepsilon_{\mathrm{eq}}.$$

Let us now indicate the modifications made by taking into account temperature variations and major transformations. It is then necessary to add the increment of thermal deformation $\Delta\varepsilon^{\mathrm{t}}$ in the second member of Eq.(28). In addition, equations Eq. (29) and Eq.(30) should be replaced by:

$$\begin{cases} \Delta\mathbf{s} + (\Delta\mathbf{s})_{\mathrm{J\ or\ M}} \equiv 2\mu'\Delta\mathbf{e}^{\mathrm{e}} + \dfrac{\Delta\mathrm{E}}{\mathrm{E}}\mathbf{s},\ (\Delta\mathbf{s})_{\mathrm{J\ or\ M}} \equiv \Sigma\cdot\Delta\boldsymbol{\Omega} - \Delta\boldsymbol{\Omega}\cdot\Sigma \\ \Delta\Sigma_{\mathrm{m}} = \left(3\lambda'+2\mu'\right)\Delta\varepsilon^{\mathrm{e}}_{\mathrm{m}} + \dfrac{\Delta\mathrm{E}}{\mathrm{E}}\Sigma_{\mathrm{m}} \end{cases} \tag{49}$$

where $\Delta\boldsymbol{\Omega} = \boldsymbol{\Omega}\Delta t$ represents the rotation increment[5]. In these equations, the Lamé coefficients λ' and μ' are taken at time $t + \Delta t$, but the Young's modulus E and the stresses $\boldsymbol{\Sigma}, \mathbf{s}, \Sigma_{\mathrm{m}}$ at the time t.

[5]Note that the expression of $\Delta\Sigma_{\mathrm{m}}$ does not include a corrective term da to the objective derivative; this is because the trace $\boldsymbol{\Sigma}\cdot\boldsymbol{\Omega} - \boldsymbol{\Omega}\cdot\boldsymbol{\Sigma}$ is zero (consequence of = $\mathbf{tr}(\mathbf{A}\cdot\mathbf{B})$= $\mathbf{tr}(\mathbf{B}\cdot\mathbf{A})$)

The approach is then the same as before, but adding $\mathbf{s} - (\Delta\mathbf{s})_{\mathrm{J\ or\ M}}$ to the two members of Eq. $(49)_1$ instead of $\mathbf{s}$; the equations obtained are the same as before provided that expressions Eq.(39) and Eq.(41) of $\mathbf{s}^*$ and Σ_{m}^* are modified as follows:

$$\begin{cases} \mathbf{s}^* = \mathbf{s} + 2\mu'\Delta\mathbf{e}^{\mathrm{e}} - (\Delta\mathbf{s})_{\mathrm{J\ or\ M}} + \dfrac{\Delta \mathrm{E}}{\mathrm{E}}\mathbf{s}, \\ \\ \Sigma_{\mathrm{m}}^* = \Sigma_{\mathrm{m}} + (3\lambda' + 2\mu')\left(\Delta E_{\mathrm{m}} - \Delta\varepsilon_{\mathrm{m}}^{\mathrm{t}}\right) + \dfrac{\Delta \mathrm{E}}{\mathrm{E}}\Sigma_{\mathrm{m}}. \end{cases} \tag{50}$$

The rest of the resolution is unchanged except for these changes (and the $\lambda \to \lambda'$ and $\mu \to \mu'$ substitutions.) In practice, the corrective terms $-(\Delta\mathbf{s})_{\mathrm{J\ or\ M}}$, $\dfrac{\Delta \mathrm{E}}{\mathrm{E}}\mathbf{s}$, $-(3\lambda' + 2\mu')\,\Delta\varepsilon^{\mathrm{t}}$ and $\dfrac{\Delta \mathrm{E}}{\mathrm{E}}\Sigma_{\mathrm{m}}$ are added to $\mathbf{s}^*$ and Σ_{m}^*.

4.3.3. Stress correction - case of kinematics hardening

The discretized equations of the problem are written here, with notations analogous to those of the isotropic case:

$$
\left\{
\begin{array}{l}
\Delta\boldsymbol{\varepsilon} = \Delta\boldsymbol{\varepsilon}^{\mathrm{e}} + \Delta\boldsymbol{\varepsilon}^{p} + \boldsymbol{\varepsilon}^{\mathrm{t}} \\
\\
\Delta\mathbf{s} + (\Delta\mathbf{s})_{\mathrm{J\ or\ M}} = 2\mu'\Delta\mathbf{e}^{\mathrm{e}} + \dfrac{\Delta \mathrm{E}}{\mathrm{E}}\mathbf{s}, \\
\\
\Delta\Sigma_{\mathrm{m}} = \left(3\lambda' + 2\mu'\right)\Delta\varepsilon_{\mathrm{m}}^{\mathrm{e}} + \dfrac{\Delta \mathrm{E}}{\mathrm{E}}\Sigma_{\mathrm{m}}
\end{array}
\right.
$$

$$
\left\{
\begin{array}{l}
\dfrac{\Sigma_{\mathrm{eq}}'^2}{\Sigma_0'^2} + 2\tilde{p}'\, ch\left(\dfrac{3}{2}\dfrac{\Sigma_{\mathrm{m}}' - \alpha_{\mathrm{m}}'}{\Sigma_0'}\right) - 1 - \tilde{p}'^2 = 0 \\
\\
\Sigma_{\mathrm{eq}}' = \left[\dfrac{3}{2}\left(s_{\mathrm{ij}}' - \mathrm{a}_{\mathrm{ij}}'\right)\left(\mathrm{s}_{\mathrm{ij}}' - \mathrm{a}_{\mathrm{ij}}'\right)\right]^{\frac{1}{2}}
\end{array}
\right.
$$

$$
\left\{
\begin{array}{l}
\Delta\mathbf{e}^{\mathrm{p}} = \dfrac{3}{2}\dfrac{\Delta\varepsilon_{\mathrm{eq}}}{\Sigma_{\mathrm{eq}}'}\left(\mathbf{s}' - \mathbf{a}'\right)\ , \\
\\
\Delta\varepsilon_{\mathrm{m}}^{\mathrm{p}} = \dfrac{\tilde{p}''}{2}\dfrac{\Sigma_0'}{\Sigma_{\mathrm{eq}}'}\, sh\left(\dfrac{3}{2}\dfrac{\Sigma_{\mathrm{m}}' - \alpha_{\mathrm{m}}'}{\Sigma_0'}\right)\Delta\varepsilon_{\mathrm{eq}}\ .
\end{array}
\right. \tag{51}
$$

$$
\left\{
\begin{array}{l}
\Delta\mathbf{a} + (\Delta\mathbf{a})_{\mathrm{J\ or\ M}} = \dfrac{2}{3}\left(\dfrac{\Delta\tilde{\alpha}_{\mathrm{eq}}}{\Delta\varepsilon_{\mathrm{eq}}}\right)_T \Delta\mathbf{e}^{\mathrm{P}} + \dfrac{1}{\tilde{\alpha}_{\mathrm{eq}}}\left(\dfrac{\Delta\tilde{\alpha}_{\mathrm{eq}}}{\Delta\theta}\right)\mathbf{a}\Delta\theta, \\
\\
(\Delta\mathbf{a})_{\mathrm{J\ or\ M}} = \mathbf{a}\cdot\Delta\Omega - \Delta\Omega\cdot\mathbf{a} \\
\\
\Delta\alpha_{\mathrm{m}} = \left(\dfrac{\Delta\tilde{\alpha}_{\mathrm{m}}}{\Delta\varepsilon_{\mathrm{m}}}\right)_T \Delta\varepsilon_{\mathrm{m}}^{\mathrm{p}} + \dfrac{1}{\tilde{\alpha}_{\mathrm{m}}}\left(\dfrac{\Delta\tilde{\alpha}_{\mathrm{m}}}{\Delta\theta}\right)\alpha_{\mathrm{m}}\Delta\theta
\end{array}
\right.
$$

$$
\left\{
\begin{array}{l}
\tilde{\alpha}_{\mathrm{eq}} \equiv \tilde{\alpha}_{\mathrm{eq}}\left(\varepsilon_{\mathrm{eq}}, \varepsilon_{\mathrm{m}}, \theta\right), \quad \tilde{\alpha}_{\mathrm{m}} \equiv \tilde{\alpha}_{\mathrm{m}}\left(\varepsilon_{\mathrm{eq}}, \varepsilon_{\mathrm{m}}, \theta\right) \\
\\
\Delta\varepsilon_{\mathrm{eq}} = \left(\dfrac{2}{3}\Delta\mathrm{e}_{\mathrm{ij}}^{\mathrm{p}}\cdot\Delta\mathrm{e}_{\mathrm{ij}}^{\mathrm{p}}\right)^{\frac{1}{2}}, \Delta\varepsilon_{\mathrm{m}} = \left|\Delta\varepsilon_{\mathrm{m}}^{\mathrm{p}}\right|
\end{array}
\right.
$$

As usual, the secants $\left(\Delta\tilde{\alpha}_{\mathrm{eq}}\middle/\Delta\varepsilon_{\mathrm{eq}}\right)_T$ and $\left(\Delta\tilde{\alpha}_{\mathrm{m}}\middle/\Delta\varepsilon_{\mathrm{m}}\right)_T$ are taken has the final temperature θ', and the secants $\left(\Delta\tilde{\alpha}_{\mathrm{eq}}\middle/\Delta\theta\right)$ and $\left(\Delta\tilde{\alpha}_{\mathrm{m}}\middle/\Delta\theta\right)$ has the initial $\left(\varepsilon_{\mathrm{eq}}, \varepsilon_{\mathrm{m}}\right)$ deformation. Moreover, the first two secants are taken at constant triaxiality equal to the initial triaxiality $T = \varepsilon_{\mathrm{m}}/\varepsilon_{\mathrm{eq}}$.

Adding $\mathbf{s} - (\Delta\mathbf{s})_{\mathrm{J\ or\ M}} - \mathbf{a} - \Delta\mathbf{a}$ to both members from Eq.(51)$_{2,3}$ we get

$$
\mathbf{s}' - \mathbf{a}' \equiv \mathbf{s} + \Delta\mathbf{s} - \mathbf{a} - \Delta\mathbf{a} = \mathbf{s} + 2\mu'\Delta\mathbf{e}^{\mathrm{e}} - (\Delta\mathbf{s})_{\mathrm{J\ or\ M}} + \frac{\Delta \mathrm{E}}{\mathrm{E}}\mathbf{s} - \mathbf{a} - \Delta\mathbf{a}
$$

which yields, taking into account Eq.(51)$_1$, Eq.(51)$_7$, Eq.(51)$_9$:

$$\mathbf{s}' - \mathbf{a}' = \mathbf{s} + 2\mu'\Delta\mathbf{e} - (\Delta\mathbf{s})_{\text{J or M}} + \frac{\Delta \text{E}}{\text{E}}\mathbf{s} - \mathbf{a} - \frac{2}{3}\left(\frac{\Delta\tilde{\alpha}_{\text{eq}}}{\Delta\varepsilon_{\text{eq}}}\right)_T \frac{3}{2}\frac{\Delta\varepsilon_{\text{eq}}}{\Sigma'_{\text{eq}}}\left(\mathbf{s}' - \mathbf{a}'\right) \tag{52}$$

$$+ (\Delta\mathbf{a})_{\text{J or M}} - \frac{1}{\tilde{\alpha}_{\text{eq}}}\left(\frac{\Delta\tilde{\alpha}_{\text{eq}}}{\Delta\theta}\right)\mathbf{a}\Delta\theta - 2\mu'\frac{3}{2}\frac{\Delta\varepsilon_{\text{eq}}}{\Sigma'_{\text{eq}}}\left(\mathbf{s}' - \mathbf{a}'\right).$$

Assuming

$$\mathbf{s}^* = \mathbf{s} + 2\mu'\Delta\mathbf{e} - (\Delta\mathbf{s})_{\text{J or M}} + \frac{\Delta \text{E}}{\text{E}}\mathbf{s} - \mathbf{a} + (\Delta\mathbf{a})_{\text{J or M}} - \frac{1}{\tilde{\alpha}_{\text{eq}}}\left(\frac{\Delta\tilde{\alpha}_{\text{eq}}}{\Delta\theta}\right)\mathbf{a}\Delta\theta \tag{53}$$

($\mathbf{s}^*$ is a known quantity), this is written

$$\mathbf{s}' - \mathbf{a}' = \mathbf{s}^* - \left[3\mu' + \left(\frac{\Delta\tilde{\alpha}_{\text{eq}}}{\Delta\varepsilon_{\text{eq}}}\right)_T\right]\frac{\Delta\varepsilon_{\text{eq}}}{\Sigma'_{\text{eq}}}\left(\mathbf{s}' - \mathbf{a}'\right) \tag{54}$$

equation which shows that $\mathbf{s}' - \mathbf{a}'$ and $\mathbf{s}^*$ are parallel and reduces, as in the isotropic case, the computation from Δep to that of $\Delta\varepsilon_{\text{eq}}$. Moreover, taking the Von Mises function of the two members, we obtain by setting

$$\Sigma^*_{\text{eq}} = \left(\frac{3}{2}\text{s}^*_{\text{ij}}\text{s}^*_{\text{ij}}\right)^{\frac{1}{2}}. \tag{55}$$

the equation

$$\Sigma^*_{\text{eq}} - \Sigma'_{\text{eq}} = \left[3\mu' + \left(\frac{\Delta\tilde{\alpha}_{\text{eq}}}{\Delta\varepsilon_{\text{eq}}}\right)_T\right]\Delta\varepsilon_{\text{eq}}, \tag{56}$$

analogous to Eq. (40) of the isotropic case.

Similarly, adding $\Sigma_{\text{m}} - \alpha_{\text{m}} - \Delta\alpha_{\text{m}}$ to both sides of Eq.(51)$_3$, we obtain :

$$\Sigma'_{\text{m}} - \alpha'_{\text{m}} \equiv \Sigma_{\text{m}} + \Delta\Sigma_{\text{m}} - \alpha_{\text{m}} - \Delta\alpha_{\text{m}} = \Sigma_{\text{m}} + \left(3\lambda' + 2\mu'\right)\Delta\varepsilon^{\text{e}}_{\text{m}} + \frac{\Delta \text{E}}{\text{E}}\Sigma_{\text{m}} - \alpha_{\text{m}} - \Delta\alpha_{\text{m}}, \tag{57}$$

which yields, taking into account Eq.(51)$_1$ and (51)$_8$:

$$\Sigma^*_{\text{m}} - (\Sigma'_{\text{m}} - \alpha'_{\text{m}}) = \left[3\lambda' + 2\mu' + \left(\frac{\Delta\tilde{\alpha}_{\text{m}}}{\Delta\varepsilon_{\text{m}}}\right)_T\right]\Delta\varepsilon^{\text{p}}_{\text{m}}, \tag{58}$$

where Σ^*_{m} denotes the (known) quantity defined by :

$$\Sigma^*_{\text{m}} = \Sigma_{\text{m}} + \left(3\lambda' + 2\mu'\right)\left(\Delta E_{\text{m}} - \Delta\varepsilon^{\text{t}}_{\text{m}}\right) + \frac{\Delta \text{E}}{\text{E}}\Sigma_{\text{m}} - \alpha_{\text{m}} - \frac{1}{\tilde{\alpha}_{\text{m}}}\left(\frac{\Delta\tilde{\alpha}_{\text{m}}}{\Delta\theta}\right)\alpha_{\text{m}}\Delta\theta; \tag{59}$$

Eq. (58) is analogous to Eq. (41) in the isotropic case. Now combining Eq.(51)$_5$, Eq.(56) and Eq.(58), we get:

$$\frac{3\mu' + \left(\frac{\Delta\tilde{\alpha}_{\text{eq}}}{\Delta\varepsilon_{\text{eq}}}\right)_T}{3\lambda' + 2\mu' + \left(\frac{\Delta\tilde{\alpha}_{\text{m}}}{\Delta\varepsilon_{\text{m}}}\right)_T}\frac{\Sigma^*_{\text{m}} - (\Sigma'_{\text{m}} - \alpha'_{\text{m}})}{\Sigma^*_{\text{eq}} - \Sigma'_{\text{eq}}} = \frac{\tilde{p}''}{2}\frac{\Sigma'_0}{\Sigma'_{\text{eq}}}sh\left(\frac{3}{2}\frac{\Sigma'_{\text{m}} - \alpha'_{\text{m}}}{\Sigma'_0}\right), \tag{60}$$

equation analogous to Eq. (44).

From there, we adopt an iterative resolution method, as in the case of isotropic work hardening starting from initial values of the parameters:

$$\Delta\varepsilon_{\rm eq},\ \Delta\varepsilon^{\rm p}_{\rm m},\ \Delta\varepsilon_{\rm m},\ \left(\frac{\Delta\tilde{\alpha}_{\rm eq}}{\Delta\varepsilon_{\rm eq}}\right)_T,\ \left(\frac{\Delta\tilde{\alpha}_{\rm m}}{\Delta\varepsilon_{\rm m}}\right)_T, \tag{61}$$

we start by solving the equations Eq.$(51)_2$ and Eq. (60) with respect to $\Sigma_{\rm eq}$ and $\Sigma'_{\rm m}-\alpha'_{\rm m}$; as these equations are identical to those Eq.(31) and Eq. (44) of the isotropic case on condition of replacing $\Sigma'_1, \Sigma'_2, 3\mu, 3\lambda+2\mu, \Sigma'_{\rm m}$ with

$$\Sigma'_0, \Sigma'_0, 3\mu' + \left(\frac{\Delta\tilde{\alpha}_{\rm eq}}{\Delta\varepsilon_{\rm eq}}\right)_T, 3\lambda + 2\mu + \left(\frac{\Delta\vec{\alpha}_{\rm m}}{\Delta\varepsilon_{\rm m}}\right)_T, \Sigma'_{\rm m} - \alpha'_{\rm m}, \tag{62}$$

it suffices to employ the same method with these substitutors; then we draw $\Delta\varepsilon_{\rm eq}, \Delta\varepsilon^{\rm p}_{\rm m}$ and $\Delta\varepsilon_{\rm m}$ from Eq. (56), Eq. (58), Eq. $(35)_2$, we deduce

$$\left(\frac{\Delta\tilde{\alpha}_{\rm eq}}{\Delta\varepsilon_{\rm eq}}\right)_T \text{ and } \left(\frac{\Delta\tilde{\alpha}_{\rm m}}{\Delta\varepsilon_{\rm m}}\right)_T \tag{63}$$

thanks to Eq. $(51)_{11}$ and we iterate the process until convergence.

When this calculation is finished, it is not only necessary to calculate, as in the isotropic case, the local increment of porosity Δf_1, but also to evolve $\mathbf{a}$ and $\alpha_{\rm m}$ according to formula Eq. $(51)_{6,7,8}$.

4.3.4. Stress correction - case of mixed isotropic / kinematic Hardening

The discretized equations of the problem are the same as in the kinematic case, with the exception of Eq. $(51)_{2,3}$ and Eq. $(51)_{4,5}$ which are written here:

$$\begin{cases} \dfrac{\Sigma'^2_{\rm eq}}{\left[\rho\Sigma'_0 + (1-\rho)\Sigma'_1\right]^2} + 2\tilde{p}' ch\left(\dfrac{3}{2}\dfrac{\Sigma'_{\rm m} - \rho\alpha'_{\rm m}}{\rho\left(\Sigma'_0 + (1-\rho)\Sigma'_2\right)}\right) - 1 - \tilde{p}^2 = 0, \\ \Sigma'_{\rm eq} \equiv \left[\dfrac{3}{2}\left(s'_{ij} - \rho a'_{ij}\right)\left(s'_{ij} - \rho a'_{ij}\right)\right]^{\frac{1}{2}}. \end{cases} \tag{64}$$

$$\begin{cases} \Delta\mathbf{e}^{\rm p} = \dfrac{3}{2}\dfrac{\Delta\varepsilon_{\rm eq}}{\Sigma'_{\rm eq}}\left(\mathbf{s}' - \rho\mathbf{a}'\right), \\ \Delta\varepsilon^{p}_{\rm m} = \dfrac{\tilde{p}''}{2}\dfrac{\left[\rho\Sigma'_0 + (1-\rho)\Sigma'_1\right]^2}{\left[\rho\Sigma'_0 + (1-\rho)\Sigma'_2\right]\Sigma'_{\rm eq}} sh\left(\dfrac{3}{2}\dfrac{\Sigma'_{\rm m} - \rho\alpha'_{\rm m}}{\left[\rho\Sigma'_0 + (1-\rho)\Sigma'_2\right]}\right)\Delta\varepsilon_{\rm eq} \end{cases} \tag{65}$$

In these equations, Σ'_1 and Σ'_2 are given by:

$$\Sigma'_1 \equiv \Sigma_1(\varepsilon'_{\rm eq}, \varepsilon'_{\rm m}, \theta'), \quad \Sigma'_2 \equiv \Sigma_2(\varepsilon'_{\rm eq}, \varepsilon'_{\rm m}, \theta').$$

We do not repeat here the whole approach and we will content ourselves with indicating how the final equations must be modified with respect to the kinematic case: Eq.(53) and Eq. (59) become

$$\mathbf{s}^* = \mathbf{s} + 2\mu'\Delta\mathbf{e} - (\Delta\mathbf{s})_{\text{J or M}} + \frac{\Delta \text{E}}{\text{E}}\mathbf{s} - \rho\mathbf{a} + \rho(\Delta \text{a})_{\text{J or M}} - \frac{1}{\tilde{\alpha}_{\text{eq}}}\left(\frac{\Delta\tilde{\alpha}_{\text{eq}}}{\Delta\theta}\right)\rho\mathbf{a}\Delta\theta \tag{66}$$

$$\Sigma^*_{\text{eq}} - \Sigma'_{\text{eq}} = \left[3\mu' + \rho\left(\frac{\Delta\tilde{\alpha}_{\text{eq}}}{\Delta\varepsilon_{\text{eq}}}\right)_T\right]\Delta\varepsilon_{\text{eq}} \tag{67}$$

and the equations Eq.(58) and Eq.(54)

$$\Sigma^*_{\text{m}} - (\Sigma'_{\text{m}} - \rho\alpha'_{\text{m}}) = \left[3\lambda' + 2\mu' + \rho\left(\frac{\Delta\tilde{\alpha}_{\text{m}}}{\Delta\varepsilon_{\text{m}}}\right)_T\right]\Delta\varepsilon^{\text{p}}_{\text{m}} \tag{68}$$

$$\Sigma^*_{\text{m}} = \Sigma_{\text{m}} + (3\lambda' + 2\mu')\left(\Delta E_{\text{m}} - \Delta\varepsilon^{\text{t}}_{\text{m}}\right) + \frac{\Delta \text{E}}{\text{E}}\Sigma_{\text{m}} - \rho\alpha_{\text{m}} - \frac{1}{\tilde{\alpha}_{\text{m}}}\left(\frac{\Delta\tilde{\alpha}_{\text{m}}}{\Delta\varepsilon_{\text{m}}}\right)\rho\alpha_{\text{m}}\Delta\theta, \tag{69}$$

and the equation Eq.(60).

$$\frac{3\mu' + \rho\left(\frac{\Delta\tilde{\alpha}_{\text{eq}}}{\Delta\varepsilon_{\text{eq}}}\right)_T}{3\lambda' + 2\mu' + \rho\left(\frac{\Delta\tilde{\alpha}_{\text{m}}}{\Delta\varepsilon_{\text{m}}}\right)_T}\frac{\Sigma^*_{\text{m}} - (\Sigma'_{\text{m}} - \rho\alpha'_{\text{m}})}{\Sigma^*_{\text{eq}} - \Sigma'_{\text{eq}}} = \frac{\tilde{p}''}{2}\frac{\left[\rho\Sigma'_0 + (1-\rho)\Sigma'_1\right]^2}{\left[\rho\Sigma'_0 + (1-\rho)\Sigma'_2\right]\Sigma'_{\text{eq}}}sh\left(\frac{3}{2}\frac{\Sigma'_{\text{m}} - \rho\alpha'_{\text{m}}}{\rho\Sigma'_0 + (1-\rho)\Sigma'_2}\right) \tag{70}$$

The system of the two equations Eq. $(51)_{2,3}$ and Eq.(60) is solved with respect to the unknowns Σ'_{eq} and $\Sigma'_{\text{m}} - \rho\alpha'_{\text{m}}$ by the same method as in the isotropic case (equations Eq.(45), Eq.(46), Eq.(47), Eq.(48)), with the substitutions

- $\Sigma'_1 \to \rho\Sigma'_0 + (1-\rho)\Sigma'_1$
- $\Sigma'_2 \to \rho\Sigma'_0 + (1-\rho)\Sigma'_2$,
- $3\mu \to 3\mu' + \rho\left(\Delta\tilde{\alpha}_{\text{eq}}/\Delta\varepsilon_{\text{eq}}\right)_T$,
- $3\lambda + 2\mu \to 3\lambda' + 2\mu' + \rho\left(\Delta\tilde{\alpha}_{\text{m}}/\Delta\varepsilon_{\text{m}}\right)_T$,
- $\Sigma'_{\text{m}} \to \Sigma'_{\text{m}} - \rho\alpha'_{\text{m}}$.

The rest of the resolution is the same as in the kinematic case. Note that in practice, the substitutions:

- $\Sigma'_1 \to \rho\Sigma'_0 + (1-\rho)\Sigma'_1$,
- $\Sigma'_2 \to \rho\Sigma'_0 + (1-\rho)\Sigma'_2$,
- $\tilde{\alpha}_{\text{eq}} \to \rho\tilde{\alpha}_{\text{eq}}$:
- $\tilde{\alpha}_{\text{m}} \to \rho\tilde{\alpha}_{\text{m}}$.

4.4. Particular Cases

The first particular case is that, classic, of the elastic unloading: if the quantity

$$\frac{\Sigma_{\rm eq}^{*2}}{\Sigma_1'^2} + 2\tilde{p}'\ sh\left(\frac{3}{2}\frac{\Sigma_{\rm m}^*}{\Sigma_2'}\right) - 1 - \tilde{p}'^2 \tag{71}$$

(or the analogous quantities if work hardening is kinematic or mixed) is negative, there is discharge, therefore $\Delta\varepsilon_{\rm eq} = \Delta\varepsilon_{\rm m}^p = \Delta\varepsilon_{\rm m} = 0, \Delta f_1 = 0$ and there is no need to perform constraint correction. The second is that of the closing of the cavities. Examining this possibility requires comparing the porosity to its initial value f_0. Given the explicit nature of the algorithm used with respect to this parameter, it makes sense to test not the true porosity f' at time $t + \Delta t$ (which is known only at the end of the computation, after the convergence of the double iterative process), but on its approximation $\tilde{f}'$ given by Eq.(36). The reclosing test is therefore the conjunction of the inequalities $\tilde{f}' \leq f_0$ and $sh < 0$, where sh denotes the hyperbolic *sine* of $\frac{3}{2}\frac{\sigma^*{\rm m}}{\sigma_2'}$ or analogous quantities. If this test is carried out, it is considered that the criterion is that of Von Mises and the flow rule, that naturally associated ($\Leftrightarrow \tilde{p}' = \tilde{p}'' = 0$ in the previous equations).

The third special case, in a way diametrically opposed to the previous one, is that of total damage, that is to say the one where the porosity becomes so high that p exceeds 1. In this case, the material is totally ruined. It is then enough, instead of performing the constraint correction as indicated above, to cancel $\mathbf{\Sigma}'$. The calculation of the evolution of the hardening parameters is not necessary, the material remaining by hypothesis ruined later[6], but it is necessary all the same to continue to calculate the local increment of porosity Δf_1, because it influences, in the event of relocation of the damage, the evolution of the porosity at the close points, the knowledge of which remains *a priori* necessary because these points may not themselves be ruined.

The last special case is that of sudden germination (decohesion of the metallic matrix around the inclusions). To treat this case, it is necessary to maintain at 0 the porosity (even, in the case of the delocalization of the damage, if that of the neighboring points already evolves) as long as the criterion Eq.(90) is not carried out. As soon as it becomes so, it is necessary to set $f = f_0$ and to continue the calculation normally.

4.5. Numerical treatment of the damage delocalization

This proceudre uses an array $\mathrm{AF(I,J)}$. The first index varies from 1 to 6, the second from 1 to the total number of Gauss points concerned by the delocalization (it identifies the Gauss point). The meanings of the different quantities $\mathrm{AF(I,J)}$ are as follows:

- $\mathrm{AF(1,\ J), AF(2,J), AF(3,J)}$: Current coordinates of Gaussian point J;
- $\mathrm{AF(4,\ J)}$: Local porosity increment (between times t and $t + \Delta t$) at the Gaussian point J;
- $\mathrm{AF(5,J)}$: Real increment (after convolution) of porosity at the Gaussian point J;
- $\mathrm{AF(6,J)}$: Gauss point weight (for integration).

[6] For this purpose, in the program, f is prevented from decreasing again if p has reached or exceeded the value 1.

The calculation procedure is as follows: at all the iterations and for all the Gauss points, the a program is used to calculate the coordinates and the weight of the Gauss point and stores them in $\mathrm{AF}(1-3,\mathrm{J})$ and $\mathrm{AF}(6,\mathrm{J})$. It also calls the a sub-program, which evaluates

the local porosity increment; the latter is stored in $\mathrm{AF}(4,\ \mathrm{J})$. Once the convergence on the nodal imbalances has been obtained, another program is called which, thanks to a double loop on the Gauss points, performs the convolution operation. The actual porosity increment at the point J, stored in $\mathrm{AF}(5,\ \mathrm{J})$, is transmitted to a program, which performs the final operation of calculating and storing the porosity at time t and $t+\Delta t$.

4.6. Correction of the mean part of the deformation rate

The first tests of the program made appear a difficulty which is not specific to the ductile fracture but arises in a general way in elastoplasticity large deformations. This difficulty consists of an inaccuracy in the calculation of the average part of the rate of total deformation (which affects, via the law of elasticity or the law of plastic flow in the case of the ductile damage, the average stress). The origin of this inaccuracy is as follows. Between two times of calculation t and $t+\Delta t$, the algorithm employed uses a formulation linearized compared to the increment of displacement $\Delta\mathbf{u}$; thus the increment of deformation is given by the formula:

$$\Delta\varepsilon_{\mathrm{ij}}=\frac{1}{2}\left(\frac{\partial\Delta\mathrm{u_i}}{\partial\mathrm{x_j}}+\frac{\partial\Delta\mathrm{u_j}}{\partial\mathrm{x_i}}\right) \tag{72}$$

where the $\mathrm{x_i}$ designate the coordinates at time $t+\Delta t$. Similarly, the average strain is taken equal to

$$\Delta E_{\mathrm{m}}=\frac{1}{3}\frac{\partial\Delta\mathrm{u_i}}{\partial\mathrm{x_i}}. \tag{73}$$

The problem stems from the fact that due to quasi-incompressibility (compressibility is only due to elasticity and possibly damage, which, at least at the beginning of mechanical history, is weak), ΔE_{m} is small compared to each of $\Delta\varepsilon_{\mathrm{ij}}$. As a result, the neglected second-order terms in the above formulas, although indeed small compared to each of $\partial\Delta\mathrm{u_i}/\partial\mathrm{x_j}$, are not small compared to the sum $\partial\Delta\mathrm{u_i}/\partial\mathrm{x_i}$, and that it is therefore illegal to delete them in the expression of ΔE_{m}.

We have therefore decided to calculate the deviatoric part $\Delta\mathbf{e}$ of the total deformation increment using a linearized formula, but its average part ΔE_{m} exactly . To do this, we evaluate the variation in volume between the instants t and $t+\Delta t$ using the exact formula:

$$\frac{\mathrm{v}}{\mathrm{v}+\Delta\mathrm{v}}=det\left(\delta_{\mathrm{ij}}-\frac{\partial\Delta\mathrm{u_i}}{\partial\mathrm{x_j}}\right) \tag{74}$$

[7] and then ΔE_{m} by

$$3\Delta E_{\mathrm{m}}=\frac{\Delta\mathrm{v}}{\mathrm{v}}=\frac{1}{det\left(\delta_{\mathrm{ij}}-\frac{\partial\Delta\mathrm{u_i}}{\partial\mathrm{x_j}}\right)}-1 \tag{76}$$

[7] It would seem more natural to use the formula instead:

$$\frac{\mathrm{v}+\Delta\mathrm{v}}{\mathrm{v}}=det\left(\delta_{\mathrm{ij}}+\frac{\partial\Delta\mathrm{u_i}}{\partial\mathrm{X_j}}\right) \tag{75}$$

where the $\mathrm{x_j}$ denote the coordinates at time t. But this would be more delicate because in practice, when passing from instant t to instant $t+\Delta t$, only the coordinates $\left(\mathrm{x_j}\right)$ at time $t+\Delta t$ (and associated shape functions), and not of those $\left(\mathrm{X_j}\right)$ at time t.

This formula, linearized with respect to $\Delta v \Big/ v$, poses no problem because $\Delta v \Big/ v$ is effectively small (only the expansion of $\Delta v \Big/ v$ to the first order according to the $\partial \Delta u_i \Big/ \partial x_j$, that the we are careful here not to perform, would pose one).

5. Numerical implementation at finite strain

Writing constitutive equations for elastic-plastic large deformation for metals requires a temporary objective derivative (i.e. independent of the two reference in which it is evaluated); this derivative intervenes on one hand in the hypo-elasticity law, and on the other one, in the case of kinematics hardening, in the evolution equation of the center of the domain of elasticity.

In the formulation adopted in many finite elements codes, the derivative chosen was the most simple one, the Jaumann Derivative, defined by (considering for example the derivative of the Cauchy stress tensor $\mathbf{\Sigma}$):

$$\hat{\mathbf{\Sigma}} = \dot{\mathbf{\Sigma}} + \mathbf{\Sigma}.\mathbf{\Omega} - \mathbf{\Omega}.\mathbf{\Sigma} \tag{77}$$

where $\mathbf{\Omega}$ defines the rate of rotation given by

$$\mathbf{\Omega} = \frac{1}{2}\left(\nabla_{\mathbf{x}}\mathbf{U} - {}^{t}\nabla_{\mathbf{x}}\mathbf{U}\right) \Leftrightarrow \mathbf{\Omega}_{ij} = \frac{1}{2}\left(\frac{\partial U_i}{\partial x_j} - \frac{\partial U_j}{\partial x_i}\right) \tag{78}$$

($\mathbf{x}$, current position vector; $\mathbf{U}$ the speed). The use of this derivative to calculate the behavior in simple shear gives rise to oscillations of the shear stress as function of the strain. Although this prediction only concerns very large deformations and, consequently, no experiment has ever come to demonstrate its unrealistic character, it is considered unsatisfactory, at least for the spirit, by many authors. It therefore seems desirable, to prevent criticism which is always possible, to offer the user of our finite element code the possibility of using another derivative not subject to this drawback.

A possible choice, suggested by Fressengeas and Molinari [16], is to adopt the Green-Naghdi derivative defined by the same formula as in Eq.(77) above, but $\mathbf{\Omega}$ being given here by

$$\mathbf{\Omega} = \dot{\mathbf{R}}.\mathbf{R}^{-1} \tag{79}$$

where $\mathbf{R}$ denotes the polar decomposition of the gradient of deformation $\mathbf{F}$. We recall that this term denotes a multiplicative decomposition of $\mathbf{F}$ of the form

$$\mathbf{F} = \mathbf{R}.\mathbf{S} \tag{80}$$

where $\mathbf{R}$ is a rotation matrix and $\mathbf{S}$ is a symmetric matrix (${}^{t}\mathbf{S} = \mathbf{S}$). Similarly, $\mathbf{F}$ admits the decomposition

$$\mathbf{F} = \tilde{\mathbf{S}}.\mathbf{R} \tag{81}$$

where $\tilde{\mathbf{S}}$ is another symmetric matrix but $\mathbf{R}$ the same rotation matrix. The matrices $\mathbf{R}, \mathbf{S}, \tilde{\mathbf{S}}$ are defined unequivocally if it is specified that they vary continuously and that at the initial time (where $\mathbf{F} = \mathbf{I}$), $\mathbf{R} = \mathbf{S} = \tilde{\mathbf{S}} = \mathbf{I}$.
We describe here the numerical implementation associated with the choice of this derivative and integrated in our finite element code.

5.1. Calculations of $\mathbf{F}^{-1}$ at the times t and $t+\Delta t$

The whole problem is to calculate the discretized Green-Naghdi rotation rate $\mathbf{\Omega}\Delta t \equiv \Delta\mathbf{\Omega} = \Delta\mathbf{R}\mathbf{R}^{-1}$ (we then deduce for example the discretized Molinari stress rate $\Delta\mathbf{\Sigma} \equiv \Delta\mathbf{\Sigma}+\mathbf{\Sigma}\Delta\mathbf{\Omega}-\Delta\mathbf{\Omega}\mathbf{\Sigma}$). This requires calculating the rotations $\mathbf{R}(t) \equiv \mathbf{R}$ and $\mathbf{R}(t+\Delta t) \equiv \mathbf{R}'$ (or $\mathbf{R}$ and $\Delta\mathbf{R} = \mathbf{R}' - \mathbf{R}$), and for this the deformation gradients $\mathbf{F}(t) \equiv \mathbf{F}$ and $\mathbf{F}(t+\Delta t) \equiv \mathbf{F}'$.

The formula giving $\mathbf{F}'$ is written:

$$\mathbf{F}' = \frac{\partial \mathrm{x}'}{\partial \mathbf{X}} = \mathbf{I} + \frac{\partial \mathrm{u}'}{\partial \mathbf{X}} \Leftrightarrow \mathrm{F}'_{\mathrm{ij}} = \delta_{\mathrm{ij}} + \frac{\partial \mathrm{u}'_{\mathrm{i}}}{\partial \mathrm{X}'_{\mathrm{j}}} \tag{82}$$

where $\mathbf{X}$ denotes the position vector at the time 0, $\mathbf{x}'$ the position vector at time $t+\Delta t$ and $\mathbf{u}'$ the displacement vector at this time ($\mathbf{u}' = \mathbf{x}' - \mathbf{X}$). However, the use of this formula poses a problem because, when going from the time t to the time $t+\Delta t$, we only have the shape functions relative to the final coordinates x'_{i} (which prohibits evaluating the derivatives with respect to the initial coordinates X_{i}). It is therefore more convenient to calculate the inverse of $\mathbf{F}'$ using the formula

$$\mathbf{F}'^{-1} = \frac{\partial \mathbf{X}}{\partial \mathrm{x}'} = \mathbf{I} - \frac{\partial \mathrm{u}'}{\partial \mathrm{x}'} \Leftrightarrow \mathrm{F}'^{-1}_{\mathrm{ij}} = \delta_{\mathrm{ij}} - \frac{\partial \mathrm{u}'_{\mathrm{i}}}{\partial \mathrm{X}'_{\mathrm{J}}} \tag{83}$$

Of course, it is in fact the discretized version of this equation that we use:

$$\mathrm{F}'^{-1}_{\mathrm{ij}} = \delta_{\mathrm{ij}} - \sum_{\mathrm{p}} \frac{\partial \mathrm{N}_{\mathrm{p}}(\mathbf{x}')}{\partial x'_{\mathrm{j}}} \mathrm{u}'_{\mathrm{i}}(\mathrm{p}) \tag{84}$$

where the sum is extended to all the nodes of the mesh to which the considered (Gaussian) point belongs, and where $\mathrm{N}_{\mathrm{p}}(\mathbf{x}')$ and $\mathbf{u}'(\mathrm{p})$ denote respectively the shape function associated with the node p and the displacement (at time $\mathrm{t}+\Delta\mathrm{t}$) of this node. The inverse of $\mathbf{F}$ can be evaluated as follows:

$$\begin{aligned} \mathbf{F}^{-1} &= \frac{\partial \mathbf{X}}{\partial \mathbf{x}} = \frac{\partial \mathbf{X}}{\partial \mathbf{x}'} . \frac{\partial \mathbf{x}'}{\partial \mathbf{x}} = \mathbf{F}'^{-1} . \left(\mathbf{I} + \frac{\partial \Delta \mathbf{u}}{\partial \mathbf{x}} \right) . \mathbf{F}'^{-1} . \left(\mathbf{I} + \frac{\partial \Delta \mathbf{u}}{\partial \mathbf{x}'} \right) \\ \Leftrightarrow F^{-1}_{\mathrm{ij}} &= F'^{-1}_{\mathrm{ik}} . \left(\delta_{\mathrm{kj}} + \frac{\partial \Delta \mathrm{u}_{\mathbf{k}}}{\partial x'_{\mathrm{j}}} \right) \end{aligned} \tag{85}$$

where $\mathbf{x}$ denotes the position vector at the time t and $\Delta\mathbf{u}$ the increment of displacement between the times t and $t+\Delta t$ ($\Delta\mathbf{u} = \mathbf{u}' - \mathbf{u}$, $\mathbf{u} \equiv$ move at the time t). The error made by replacing $\partial\Delta\mathbf{u}\big/\partial\mathbf{x}$ by $\partial\Delta\mathbf{u}\big/\partial\mathbf{x}'$ is negligible because of the second order in Δt whereas the algorithm used is of the first order. The derivatives $\partial\Delta\mathbf{u}_{\mathrm{k}}\big/\partial\mathbf{x}'_{\mathrm{j}}$ are of course still evaluated here using the gradients of the shape functions (relative to the coordinates $\mathbf{x}'_{\mathrm{i}}$).

5.2. Two Dimensional Case

We must now calculate $\mathbf{R}$ and $\mathbf{R}'$, or $\mathbf{R}$ and $\Delta\mathbf{R}$, and the discretized rotation rate $\Delta\mathbf{\Omega}$. We are going to distinguish here the two-dimensional and three-dimensional cases, because we will not proceed in the same way in the two cases (direct calculation of $\mathbf{R}$ and $\mathbf{R}$ without storage in the two-dimensional case, calculation of $\mathbf{R}$ and $\Delta\mathbf{R}$ with storage of $\mathbf{R}$ in the three-dimensional case). Let us consider first the two-dimensional case.

Since we do not know $\mathbf{F}$ and $\mathbf{F}'$ directly but their inverses, it is convenient to consider the polar decompositions of these inverses:

$$\mathbf{F}^{-1} = \mathcal{R}.\mathcal{S} = \tilde{\mathcal{S}}.\mathcal{R},\ \mathbf{F}'^{-1} = \mathcal{R}'.\mathcal{S}' = \tilde{\mathcal{S}}'.\mathcal{R}' \tag{86}$$

where $\mathcal{R}$ and $\mathcal{R}'$ are the rotation matrices, $\mathcal{S}, \tilde{\mathcal{S}}, \mathcal{S}', \tilde{\mathcal{S}}'$ symmetric matrices . The quantities $\mathcal{R}$ and $\mathcal{R}'$ are none other than the inverses of $\mathbf{R}$ and $\mathbf{R}'$: indeed, for $\mathbf{F}$ for example, we have:

$$\mathbf{F}^{-1} = \tilde{S}.\mathcal{R} \Rightarrow \mathbf{F} = R^{-1}.\tilde{\mathcal{S}}^{-1}; \tag{87}$$

the comparison with Eq.(81) and the uniqueness of $\mathcal{R}$ and $\mathcal{S}$ show that $\mathcal{R}^{-1} = \mathbf{R}$. If we know how to calculate $\mathcal{R}$ and $\mathcal{R}'$, we can easily deduce the discretized rotation rate:

$$\Delta\mathbf{\Omega} = \Delta\mathbf{R}.\mathbf{R}^{-1} \cong \Delta\mathbf{R}.\mathbf{R}'^{-1} = (\mathbf{R}' - \mathbf{R}).\mathbf{R}'^{-1} = \mathbf{1} - \mathbf{R}.\mathbf{R}'^{-1} = \mathbf{1} - \mathcal{R}^{-1}.\mathcal{R}'. \tag{88}$$

The problem is therefore reduced to the calculation of the rotations $\mathcal{R}$ and $\mathcal{R}'$ or to that, equivalent, of the matrices $\mathcal{S}$ and $\mathcal{S}'$, of the polar decompositions of $\mathbf{F}^{-1}$ and $\mathbf{F}'^{-1}$. Consider for example that of $\mathbf{F}^{-1}$. Let us introduce the matrix of dilatations (symmetric and known)

$$C = {}^t\mathbf{F}^{-1}.\mathbf{F}^{-1}. \tag{89}$$

Thus, we have

$$C = {}^t(\mathcal{R}.\mathcal{S}).\mathcal{R}.\mathcal{S} = {}^t\mathcal{S}{}^t\mathcal{R}.\mathcal{R}.\mathcal{S} = \mathcal{S}^2. \tag{90}$$

Thus $\mathcal{S}$ appears as the square root of C. This square root is uniquely defined given the requirements that it is symmetric, a continuous function of time (like C) and identical to the identity at the initial time. Let assume that :

$$C = \begin{bmatrix} \mathrm{a} & \mathrm{b} \\ \mathrm{b} & \mathrm{c} \end{bmatrix};\ \mathcal{S} = \begin{bmatrix} \alpha & \beta \\ \beta & \gamma \end{bmatrix} \tag{91}$$

The matrix equation $C = \mathcal{S}^2$ is then written:

$$\begin{cases} \alpha^2 + \beta^2 & = \mathrm{a} \\ \beta(\alpha + \gamma) & = \mathrm{b}\ . \\ \beta^2 + \gamma^2 & = \mathrm{c} \end{cases} \tag{92}$$

In addition, the matrix equation $C = (det(\mathcal{S}))^2$ is then written as:

$$\Delta \equiv \mathrm{ac} - \mathrm{b}^2 = (\alpha\gamma - \beta)^2 \Rightarrow \alpha\gamma - \beta^2 = \sqrt{\Delta}, \tag{93}$$

the choice of the sign in front of the radical results from the continuity and that initially, $\Delta = 1, \alpha = \gamma = 1, \beta = 0$. Adding this result to Eq.(B.2)$_1$ on one hand, Eq.(B.2)$_3$ on the other hand, we obtain:

$$\begin{cases} \alpha(\alpha + \gamma) = \mathrm{a} + \sqrt{\Delta} \\ \gamma(\alpha + \gamma) = \mathrm{c} + \sqrt{\Delta} \end{cases} \tag{94}$$

the addition of these equations gives $(\alpha+\gamma)^2 = \mathrm{a}+\mathrm{c}+2\sqrt{\Delta}$, i.e. $\alpha+\gamma = \sqrt{\mathrm{a}+\mathrm{c}+2\sqrt{\Delta}}$ given that initially, $\mathrm{a}=\mathrm{c}=1, \Delta=1, \alpha=\gamma=1$. Transferring this result to Eq.(B.5) and Eq.(B.2)$_2$, we finally obtain:

$$\begin{cases} \alpha = \dfrac{\mathrm{a}+\sqrt{\Delta}}{\sqrt{\mathrm{a}+\mathrm{c}+2\sqrt{\Delta}}} \\ \beta = \dfrac{\mathrm{b}}{\sqrt{\mathrm{a}+\mathrm{c}+2\sqrt{\Delta}}} \\ \gamma = \dfrac{\mathrm{c}+\sqrt{\Delta}}{\sqrt{\mathrm{a}+\mathrm{c}+2\sqrt{\Delta}}} \end{cases} \tag{95}$$

These equations allow the calculation of $\mathcal{S}$ as a function of C. The expression of $\mathcal{R}$ follows immediately thanks to the formula $\mathcal{R} = \mathbf{F}^{-1}.\mathcal{S}^{-1}$.

5.3. The Three Dimensional Case

We have seen, in the two-dimensional case, that the calculation of $\mathcal{R}$ or $\mathcal{S}$ is equivalent to that of the square root of C, itself fundamentally equivalent to the diagonalization of this matrix. In the two-dimensional case, this results in painless extractions of square roots. In the three-dimensional case, it is a question of solving an equation of the 3^{rd} degree, which is more unpleasant and costly in computing time. We therefore use another, faster method, consisting of an incremental calculation of $\mathbf{R}$ (and $\mathbf{R}'$) and requiring storage, Gauss point by Gauss point , of $\mathbf{R}$. This method would indeed also lead to faster calculations in the two-dimensional case, but its use is not possible in this case because of the need to store $\mathbf{R}$.

5.3.1. Calculation of the rotation from the rotation vector

In fact, the storage of the rotation matrix itself is less economical (9 quantities to store) and redundant, the coefficients being related due to the relationship ${}^t\mathbf{R}.\mathbf{R} = \mathbf{R}.{}^t\mathbf{R} = \mathbf{I}$. The most economical way to proceed[8] consists in storing the 3 components of the rotation vector $\mathbf{V}$ defined by:

$$\mathbf{V} = \Theta\mathbf{v} \tag{96}$$

where Θ denotes the angle of rotation and $\mathbf{v}$ the unit vector parallel with the axis of rotation. Θ is a priori defined modulo 2π, but it is obvious that we can change the sign of Θ and $\mathbf{v}$ without modifying $\mathbf{R}$; there is therefore uniqueness of Θ and $\mathbf{v}$ only if it is specified that Θ is in the interval $[0,\pi]$.

The first problem that arises is therefore to reconstruct the rotation matrix $\mathbf{R}$ from the rotation vector $\mathbf{V}$. For this, let us calculate the image, by the rotation $\mathbf{R}$, of any vector $\mathbf{W}$. The projection of $\mathbf{W}$ on the axis of rotation

[8] A classic method is to store the quaternion associated with the rotation; but this quaternion has 4 components instead of 3.

is $(\mathbf{v}.\mathbf{W})\,\mathbf{v} = \dfrac{1}{\Theta^2}\,(\mathbf{V}.\mathbf{W})\,\mathbf{V}$; this projection is rotation invariant. The projection of $\mathbf{W}$ on the plane perpendicular to the axis of rotation is $\mathbf{W}' = \mathbf{W} - \frac{1}{\Theta^2}(\mathbf{V}.\mathbf{W})\mathbf{V}$; after rotation, this projection becomes:

$$cos\Theta\mathbf{W}' + sin\Theta\mathbf{v}\wedge\mathbf{W}' = cos\Theta\left[\mathbf{W} - \frac{1}{\Theta^2}(\mathbf{V}.\mathbf{W})\mathbf{V}\right] + \frac{sin\Theta}{\Theta}\mathbf{V}\wedge\left[\mathbf{W} - \frac{1}{\Theta^2}(\mathbf{V}.\mathbf{W})\mathbf{V}\right] \tag{97}$$

$$\tag{98}$$

$$= cos\Theta\left[\mathbf{W} - \frac{1}{\Theta^2}(\mathbf{V}.\mathbf{W})\mathbf{V}\right] + \frac{sin\Theta}{\Theta}\mathbf{V}\wedge\mathbf{W}. \tag{99}$$

In total, $\mathbf{W}$ thus becomes, after rotation,

$$\mathbf{RW} = \frac{1-cos\Theta}{\Theta^2}(\mathbf{V}.\mathbf{W})\mathbf{V} + cos\,\Theta\mathbf{W} + \frac{sin\Theta}{\Theta}\mathbf{V}\wedge\mathbf{W}. \tag{100}$$

The components of $\mathbf{R}$ are therefore given, given that $(\mathbf{V}\wedge\mathbf{W})_i = \varepsilon_{ikj}.V_kW_j$ where ε denotes the permutation tensor (completely anti-symmetric), by the formula:

$$R_{ij} = \frac{1-cos\Theta}{\Theta^2}V_iV_j + cos\Theta\delta_{ij} + \frac{sin\Theta}{\Theta}\varepsilon_{ikj}V_k, \Theta \equiv \|\mathbf{V}\| \tag{101}$$

5.4. Calculation of the discretized rate of rotation vector

We now come to the central problem, which is to calculate, from the knowledge of $\mathbf{R}, \mathbf{F}^{-1}, \mathbf{F}'^{-1}$, the discretized rotation rate $\Delta\mathbf{\Omega} = \mathbf{\Delta R}.\mathbf{R^{-1}}$, or rather the associated discretized rotation rate vector $\Delta\omega$, defined by:

$$\forall\mathbf{W}:\ \Delta\Omega.\mathbf{W} = \Delta\omega\wedge\mathbf{W} \tag{102}$$

To some terms in $(\Delta t)^2$, $\Delta\omega = \mathbf{\dot{R}}.\mathbf{R^{-1}}$ is anti-symmetric; to any such matrix $\mathbf{A}$ is associated a vector a such that $\forall\mathbf{W}, \mathbf{A}.\mathbf{W} = \mathbf{a}\wedge\mathbf{W}$.

From $\mathbf{R}, \mathbf{F}^{-1}, \mathbf{F}'^{-1}$, we easily form the matrices

$$\begin{cases} \Delta\mathbf{M} = \mathbf{R}.\left(\mathbf{F}^{-1} - \mathbf{F}'^{-1}\right) \\ \tilde{\mathbf{S}}^{-1} = \mathbf{R}.\mathbf{F}^{-1} \end{cases} \tag{103}$$

($\tilde{\mathbf{S}}^{-1}$ is none other than the inverse of the matrix $\tilde{\mathbf{S}}$ of the polar decomposition Eq.(81)'). Let $\Delta\tilde{\mathbf{S}} = \tilde{\mathbf{S}}' - \tilde{\mathbf{S}}$, where $\tilde{\mathbf{S}}'^{-1}$ denotes the symmetric matrix of the polar decomposition Eq.(81)) at the time $t + \Delta t$.
We have

$$\tilde{\mathbf{S}}'^{-1} = (\tilde{\mathbf{S}} + \Delta\tilde{\mathbf{S}})^{-1} = \left[\tilde{\mathbf{S}}.\left(\mathbf{I} + \tilde{\mathbf{S}}^{-1}.\Delta\tilde{\mathbf{S}}\right)\right]^{-1} \cong \left(\mathbf{I} - \tilde{\mathbf{S}}^{-1}.\Delta\tilde{\mathbf{S}}\right)\tilde{\mathbf{S}}^{-1} \tag{104}$$

Therefore:

$$\begin{aligned} \Delta\mathbf{M} = \mathbf{R}.\left(\mathbf{F}^{-1} - \mathbf{F}'^{-1}\right) &= \mathbf{R}.\left[{}^t\mathbf{R}.\tilde{\mathbf{S}}^{-1} - \left({}^t\mathbf{R} + {}^t\Delta\mathbf{R}\right)\left(\tilde{\mathbf{S}}^{-1} - \tilde{\mathbf{S}}^{-1}\Delta\tilde{\mathbf{S}}.\tilde{\mathbf{S}}^{-1}\right)\right] \\ &\cong \mathbf{R}.\left({}^t\mathbf{R}.\tilde{\mathbf{S}}^{-1}\Delta\tilde{\mathbf{S}}.\tilde{\mathbf{S}}^{-1} - {}^t\Delta\mathbf{R}.\tilde{\mathbf{S}}^{-1}\right) \\ &= \tilde{\mathbf{S}}^{-1}.\Delta\tilde{\mathbf{S}}.\tilde{\mathbf{S}}^{-1} - \mathbf{R}{}^t\Delta\mathbf{R}.\tilde{\mathbf{S}}^{-1} \\ &= \tilde{\mathbf{S}}^{-1}.\Delta\tilde{\mathbf{S}}.\tilde{\mathbf{S}}^{-1} + \Delta\mathbf{\Omega}.\tilde{\mathbf{S}}^{-1} \end{aligned} \tag{105}$$

As a consequence

$$\Delta\mathbf{M} - {}^t\Delta\mathbf{M} = \Delta\mathbf{\Omega}.\mathbf{S}^{-1} + \tilde{\mathbf{S}}^{-1}.\Delta\mathbf{\Omega} \tag{106}$$

Let $\Delta\mathbf{m}$ be the (known) vector associated with the anti-symmetric matrix $\Delta\mathbf{M} - {}^t\Delta\mathbf{M}$. We then have $\Delta M_{ij} - \Delta M_{ji} = \varepsilon_{ikj}\Delta m_k$, and likewise $\Delta\Omega_{ij} = \varepsilon_{ikj}\Delta\omega_k$. The previous equation is therefore written as:

$$\varepsilon_{ikj}\Delta m_k = \Delta\Omega_{ik}\tilde{S}^{-1}_{kj} + \tilde{S}^{-1}_{ik}\Delta\Omega_{kj} = \varepsilon_{ilk}\Delta\omega_l\tilde{S}^{-1}_{kj} + \tilde{S}^{-1}_{ik}\varepsilon_{klj}\Delta\omega_l \tag{107}$$

Multiplying on the right and on the left by ε_{ijp} we obtain

$$\begin{aligned}
\varepsilon_{ikj}\varepsilon_{ijp}\Delta m_k &= -\varepsilon_{ijk}\varepsilon_{ijp}\Delta m_k = -2\delta_{kp}\Delta m_k = -2\Delta m_p \\
&= \varepsilon_{ilk}\varepsilon_{ijp}\Delta\omega_l\tilde{S}^{-1}_{kj} + \varepsilon_{klj}\varepsilon_{ijp}\tilde{S}^{-1}_{ik}\Delta\omega_l \\
&= \left(\delta_{lj}\delta_{kp} - \delta_{lp}\delta_{kj}\right)\tilde{S}^{-1}_{kj}\Delta\omega_l + \left(\delta_{kp}\delta_{li} - \delta_{ki}\cdot\delta_{lp}\right)\tilde{S}^{-1}_{ik}\Delta\omega_l \\
&= \tilde{S}^{-1}_{pj}\Delta\omega_j - \tilde{S}^{-1}_{jj}\Delta\omega_p + \tilde{S}^{-1}_{ip}\Delta\omega_i - \tilde{S}^{-1}_{ii}\Delta\omega_p \\
&= 2\tilde{S}^{-1}_{pj}\Delta\omega_j - 2\tilde{S}^{-1}_{jj}\Delta\omega_p \\
&\Rightarrow \Delta m_p = \left[\left(\mathrm{tr}\tilde{\mathbf{S}}^{-1}\right)\delta_{pj} - \tilde{S}^{-1}_{pi}\right]\Delta\omega_j,
\end{aligned} \tag{108}$$

This can be written as:

$$\Delta\mathbf{m} = \left[\left(\mathrm{tr}\tilde{\mathbf{S}}^{-1}\right)\mathbf{I} - \tilde{\mathbf{S}}^{-1}\right].\Delta\omega \tag{109}$$

Thus we can obtain the discretized rotation rate vector $\Delta\omega$ from $\Delta\mathbf{m}$ (i.e. $\Delta\mathbf{M}$) by simply inverting a matrix 3×3 (which is much less expensive in calculation time than a diagonalization):

$$\Delta\omega = \left[\left(\mathrm{tr}\tilde{\mathbf{S}}^{-1}\right)\mathbf{I} - \tilde{\mathbf{S}}^{-1}\right].\Delta\mathbf{m}. \tag{110}$$

We then easily deduce the discretized rotation rate $\Delta\Omega$ by the formula $\Delta\mathbf{\Omega}_{ij} = \varepsilon_{ikj}\Delta\omega_k$.

5.4.1. Calculation of the rate of the rotation vector

The vector $\Delta\omega$ being known, it is necessary to calculate and store the rotation $\mathbf{R} + \Delta\mathbf{R}$ at the time t, or more precisely the vector of rotation $\mathbf{V} + \Delta\mathbf{V}$ at this time t.

An additional advantage here is storing $\mathbf{V} + \Delta\mathbf{V}$ rather than $\mathbf{R} + \Delta\mathbf{R}$. In the second case, since the step Δt is not, numerically, infinitely small, the calculation of $\Delta\mathbf{R}$ inevitably leads to a matrix $\mathbf{R} + \Delta\mathbf{R}$ which is no longer strictly orthogonal. In the first, on the contrary, regardless of the vector $\mathbf{V} + \Delta\mathbf{V}$ calculated, the use, at the next time step, of the formula Eq.(B.5)with this rotation vector leads to a strictly orthogonal matrix.

To calculate $\Delta\mathbf{V}$, let us rewrite Eq.(B.4) with the unit vector $\mathbf{W}$ instead of the vector $\mathbf{V} = \Theta\mathbf{v}$, and differentiate it with respect to time, $\mathbf{W}$ being assumed fixed:

$$\begin{aligned}
&\mathbf{R}.\mathbf{W} = (1 - cos\Theta)(\mathbf{v}.\mathbf{W})\mathbf{v} + (cos\Theta\mathbf{W} + sin\Theta\mathbf{v}\wedge\mathbf{W}) \\
&\quad\Rightarrow \Delta\mathbf{R}.\mathbf{W} = \Delta\Theta sin\Theta(\mathbf{v}.\mathbf{W})\mathrm{v} + (1 - cos\Theta)(\Delta\mathbf{v}.\mathbf{W})\mathrm{v} + (1 - cos\Theta)(\mathbf{v}.\mathbf{W})\Delta\mathbf{v} \\
&\quad - \Delta\Theta sin\Theta\mathbf{W} + \Delta\Theta cos\Theta\mathbf{v}\wedge\mathbf{W} + sin\Theta\Delta\mathbf{v}\wedge\mathbf{W}
\end{aligned}$$

Let us apply this relation to the vector $\mathbf{W} = \mathbf{v}$ as $\Delta \mathrm{v}.\mathrm{v} = 0$ (v being unitary at any time), we obtain:

$$\begin{aligned}\Delta\mathbf{R}\mathbf{v} &= \Delta\Theta.sin\Theta\mathbf{v} + (1 - cos\Theta)\Delta\mathbf{v}.\Delta\Theta.sin\Theta\mathbf{v} + \sin\Theta(\Delta\mathbf{v}) \wedge \mathrm{v} \\ &= (1 - cos\Theta)\Delta\mathbf{v} + sin\Theta(\Delta\mathbf{v}) \wedge \mathbf{v}\end{aligned}$$

Now, for any vector $\mathbf{W}$, we have $\Delta\mathbf{R}.\mathbf{R}^{-1}\ \mathbf{W} = \Delta\Omega.\mathbf{W} = \Delta\omega \wedge \mathbf{W}$. For $\mathbf{W} = \mathbf{v}$, we have $\mathbf{R}^{-1}.\mathrm{v} = \mathrm{v}$ ($\mathbf{v}$ is carried by the axis of rotation) and therefore $\Delta\mathbf{R}.\mathbf{v} = \Delta\omega \wedge \mathbf{v}$. The previous equation is therefore written as:

$$\Delta\omega \wedge \mathbf{v} = (1 - cos\Theta)\Delta\mathbf{v} + sin\Theta\,(\Delta\mathbf{v}) \wedge \mathbf{v}. \tag{111}$$

Let us take the cross product of this equation and the vector v; taking into account the formula of the double cross product, we obtain:

$$(\Delta\omega.\mathbf{v})\mathbf{v} - \Delta\omega = (1 - cos\Theta)(\Delta\mathbf{v}) \wedge \mathbf{v} - sin\Theta\Delta\mathbf{v}. \tag{112}$$

So we have both:

$$\begin{cases} (1 - cos\Theta)\Delta\mathbf{v} + sin\Theta\,(\Delta\mathbf{v}) \wedge \mathbf{v} = \Delta\omega \wedge \mathbf{v} \\ -\sin\Theta\Delta\mathbf{v} + (1 - cos\Theta)(\Delta\mathbf{v}) \wedge \mathbf{v} = (\Delta\omega.\mathbf{v})\mathbf{v} - \Delta\omega \end{cases} \tag{113}$$

Solving this system with respect to the unknown quantity $\Delta\mathrm{v}$ and $(\Delta\mathbf{v}) \wedge \mathbf{v}$ immediately gives:

$$\begin{aligned}\Delta\mathbf{v} &= \frac{1}{2}\Delta\omega \wedge \mathbf{v} + \frac{sin\Theta}{2(1 - cos\Theta)}\Delta\omega - \frac{sin\Theta}{2(1 - cos\Theta)}(\Delta\omega.\mathbf{v})\mathbf{v} \\ &= \frac{1}{2}\Delta\omega \wedge \mathbf{v} + \frac{1 + cos\Theta}{2sin\Theta}\Delta\omega - \frac{1 + cos\Theta}{2sin\Theta}(\Delta\omega.\mathbf{v})\mathbf{v}\end{aligned} \tag{114}$$

Note that we were thus able to evaluate $\Delta\mathbf{v}$ without calculating $\Delta\Theta$. However, it is $\Delta\mathbf{V}$, and not $\Delta\mathbf{v}$, that we want to know; as $\mathbf{V} = \Theta\mathbf{v}$, we have

$$\Delta\mathbf{V} = \Delta\Theta\mathbf{v} + \Theta\Delta\mathbf{v} = \frac{\Delta\Theta}{\Theta}\mathbf{V} + \frac{1}{2}\Delta\omega \wedge \mathbf{V} + \frac{\Theta(1 + cos\Theta)}{2sin\Theta}\Delta\omega - \frac{1 + cos\Theta}{2\Theta sin\Theta}(\Delta\omega.\mathbf{V})\mathbf{V}. \tag{115}$$

To calculate $\Delta\Theta$ as a function of $\Delta\omega$, note that Eq.(B.5) implies that $tr\mathbf{R} = 1 + 2cos\Theta$; thus, $tr(\Delta\mathbf{R}) = -2\Delta\Theta sin\Theta$. But $\left(\Delta\mathbf{R}.\mathbf{R}^{-1}\right)_{\mathrm{ij}} = \Delta\Omega_{\mathrm{ij}} = \varepsilon_{\mathrm{ikj}}\Delta\omega_{\mathbf{k}}$. From there we get

$$\begin{aligned}\Delta\mathrm{R}_{\mathrm{il}} &= \left(\Delta\mathbf{R}.\mathbf{R}^{-1}\right)_{\mathrm{ij}}\mathrm{R}_{\mathrm{j1}} = \varepsilon_{\mathrm{ikj}}\Delta\omega_{\mathrm{k}}\mathrm{R}_{\mathrm{j1}} \\ &\Rightarrow \mathrm{tr}(\Delta\mathbf{R}) = \Delta\mathrm{R}_{\mathrm{ii}} = \varepsilon_{\mathrm{ikj}}\Delta\omega_{\mathrm{k}}\left(\frac{1 - cos\Theta}{\Theta^2}\mathrm{V}_{\mathrm{j}}\mathrm{V}_{\mathrm{i}} + cos\Theta\delta_{\mathrm{ji}} + \frac{sin\Theta}{\Theta}\varepsilon_{\mathrm{jmi}}\mathrm{V}_{\mathrm{m}}\right) \\ &= \varepsilon_{\mathrm{ikj}}\varepsilon_{\mathrm{jmi}}\frac{sin\Theta}{\Theta}\Delta\omega_{\mathrm{k}}\mathrm{V}_{\mathrm{m}} = -2\delta_{\mathrm{km}}\frac{sin\Theta}{\Theta}\Delta\omega_{\mathrm{k}}\mathrm{V}_{\mathrm{m}} = -2\frac{sin\Theta}{\Theta}\Delta\omega.\mathbf{V};\end{aligned} \tag{116}$$

where

$$\Delta\Theta = \frac{1}{\Theta}\Delta\omega.\mathbf{V} \tag{117}$$

Transferring this result to the previous expression of $\Delta\mathbf{V}$, we finally get

$$\Delta\mathbf{V} = \frac{1}{2}\Delta\omega \wedge \mathbf{V} + \frac{\Theta\,(1 + cos\Theta)}{2sin\Theta}\Delta\omega + \left[\frac{1}{\Theta^2} - \frac{1 + cos\Theta}{2\Theta sin\Theta}\right](\Delta\omega.\mathbf{V})\mathbf{V} \tag{118}$$

This formula allows the incrementation of the vector $\mathbf{V}$. If, after the incrementation, the norm of this vector exceeds π, we correct this last modulo $2\pi\mathbf{v}$, i.e. we perform the substitution

$$\mathbf{V} \rightarrow \mathbf{V} - 2\pi\mathbf{v} = \left(1 - \frac{2\pi}{||\mathbf{V}||}\right)\mathbf{V} \tag{119}$$

(which is equivalent to replacing θ by $2\pi - \Theta$ and $\mathbf{v}$ by - $\mathbf{v}$).

5.5. Example: simple shear

We consider the typical example of a rigid plastic material, with linear kinematic work hardening, subjected to a stress of simple shear. The relations between the initial coordinates $\mathrm{X_i}$ and current coordinates $\mathrm{x_i}$ are written, for this load.

$$\begin{cases} \mathrm{x_1} = \mathrm{X_1} + \gamma\mathrm{X_2} \\ \mathrm{x_2} = \mathrm{X_2} \\ \mathrm{x_3} = \mathrm{X_3} \end{cases} \tag{120}$$

The expression of the shear stress $\tau \equiv \Sigma_{12}$ as a function of the deformation parameter γ is given by FRESSEENEAS and MOLINARI [17].

$$\tau = \frac{\Sigma_0}{\sqrt{3}} + \frac{h}{3}\left[\frac{2\gamma}{1 + \gamma^2/4}ln\left(1 + \gamma^2/4\right) + \frac{1 - \gamma^2/4}{1 + \gamma^2/4}\left(-\gamma + 4Arctg\frac{\gamma}{2}\right)\right], \tag{121}$$

where Σ_0 and h denotes the initial elastic limit and the slope of work hardening in a simple tensile test. Fig.(1) shows the comparison of the results obtained numerically (with $\Sigma_0 = 500, h = 1000$ and $\mathrm{E} = 2000000$: quasi-rigid material) and those deduced from the formula Eq.(121). The agreement is excellent.

We also compared the theoretical and numerical values of Σ_{11}; the agreement is again excellent. The above comparison is for the two-dimensional option; a comparable agreement is obtained in the three-dimensional option, but not shown here.

6. Applications

6.1. Generalities

We will simulate Mudry's [19] fracture test on a pre-notched and pre-cracked round bar (TA30) made of A508 Class 3 or 16MND5 steel. The available experimental results for comparison concern the low-alloy steel 16MND5, which is used in the fabrication of nuclear reactor vessels. For this steel, the Young's modulus is $E = 203,000$ MPa, the Poisson's ratio is $\nu = 0.3$, and the initial yield strength in uniaxial tension is $\sigma_y = 450$ MPa.

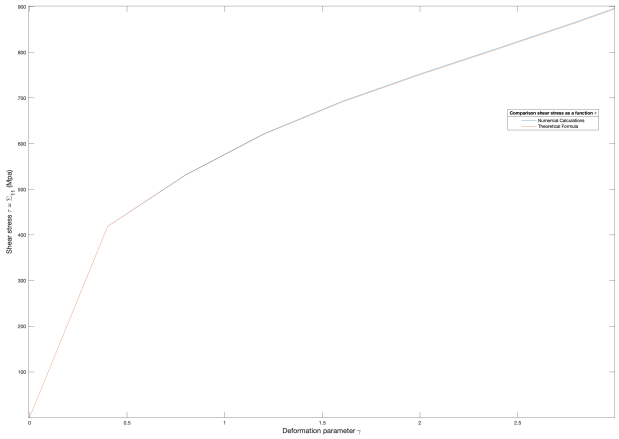

Figure 1: Shear stress as a function of the deformation parameter

Numerical simulations were carried out using the finite element code Systus®. In each simulation, the value of the Tvergaard parameter $q = 4/e = 1.47$ was used, as determined by Perrin and Leblond [5] using a "differential" scheme. The other damage parameters depend on the considered material and will be provided later.

The objectives of these simulations, let us recall, are twofold: first, to verify the independence of the numerical results with respect to spatial discretization, and second, to study the practical effectiveness of isotropic and kinematics methods in terms of its ability to reproduce experimental results.

The constitutive relationship of this material is deduced from rational stress-strain curves. The stress-strain curve at 100° C is well represented by the empirical law:

$$\sigma = 795\varepsilon_p^{0.01},$$

as schematically shown in Figure [2]. The elastic part is not represented as it can be neglected without significantly affecting the overall mechanical behavior of the material. The initial porosity value, denoted as f_0, for this steel is determined based on a study conducted by Murdy and Rousselier [19], which takes into account the chemical composition and inclusion state. This value is derived from the sulfur and manganese content of the material as well as the average dimensions of the inclusions. The determined value is 0.00016.

Additionally, three damage parameters are included: f_c representing the "critical" porosity for the onset of coalescence, δ as the accelerator factor for cavity growth, and b as the value of the characteristic length scale. These parameters can be adjusted for each simulation, and their respective values are listed in Table A.1.

Depending on the specific case, either isotropic, kinematic, or mixed isotropic-kinematic hardening will be employed to model the inelastic behavior. For one-off or pulsating loading cases, isotropic hardening is considered appropriate and relatively straightforward to implement in a model. In contrast, kinematic hardening models allow for the simulation of fully cyclic behavior but do not account for cyclic hardening and softening effects. If these factors are significant, it is recommended to use mixed-mode or combined models, as they

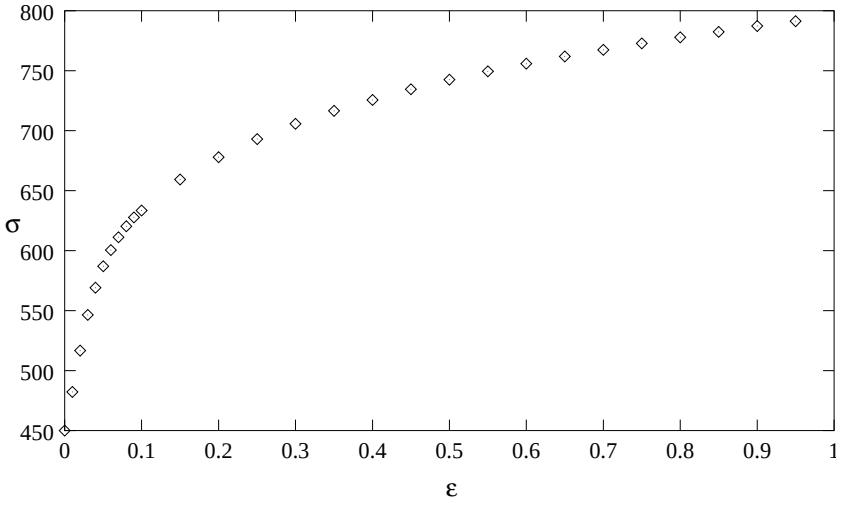

Figure 2: *Experimental stress vs. strain curve for the 16 MND5 steel*

offer the inclusion of these effects in the constitutive material behavior, providing a more comprehensive representation of the physical phenomena.

Due to the limited availability of experimental data for the steels under investigation in these studies, our focus will be solely on isotropic hardening, as it is the only approach for which experimental data are available.

Achieving convergence for the global elasto-plastic iterations posed challenges. In order to maintain the quadratic convergence rate of the global Newton iterations, it becomes necessary to incorporate stiffness tangent moduli, especially for last scale fracture problem simulations. The calculation of these tangent moduli is a highly intricate endeavor, particularly when dealing with constitutive models of complex nature. The derivation of these moduli are provided in Appendix B for both the Gurson model and the Perrin's models.

6.2. Simulation of a tensile axi-symmetric pre-notched and pre-cracked specimen.

The simulation focuses on the upper half of the specimen, taking advantage of symmetry about the horizontal mid-plane. The mesh's left boundary coincides with the axis of rotational symmetry. The specimen has a height of 90 mm and a diameter of 30 mm. The triangular central notch at the bottom of the mesh has an opening angle and depth of 60° and 5 mm, respectively. A fatigue pre-crack measuring 1.7 mm originates from the notch root. From the tip of this pre-crack, a crack develops and propagates towards the axis of rotational symmetry.

A general mesh of this specimen is shown in Figure 3. Advantage is taken of symmetry about the horizontal mid-plane to mesh only the upper half of the structure. Figure 4 shows enlarged views of the central region of the specimen. Near the crack tip of the initial fatigue pre-crack, identical discretizations are used to ensure consistent representation of the initial blunting of the crack. This avoids introducing irrelevant differences in the load-displacement curves that could interfere with the study of mesh sensitivity (for instance) due to the constitutive model's softening behavior.

To refine the modeling of intense stress and strain gradients in the crack tip region, a radiant mesh design consisting of four meshes is utilized. These four meshes employ two degenerated quadrilateral elements and two triangular elements, with their intermediate nodes pulled back to a quarter of the distance from the element face. The role of the quadrilateral elements is to facilitate crack tip opening and propagation.

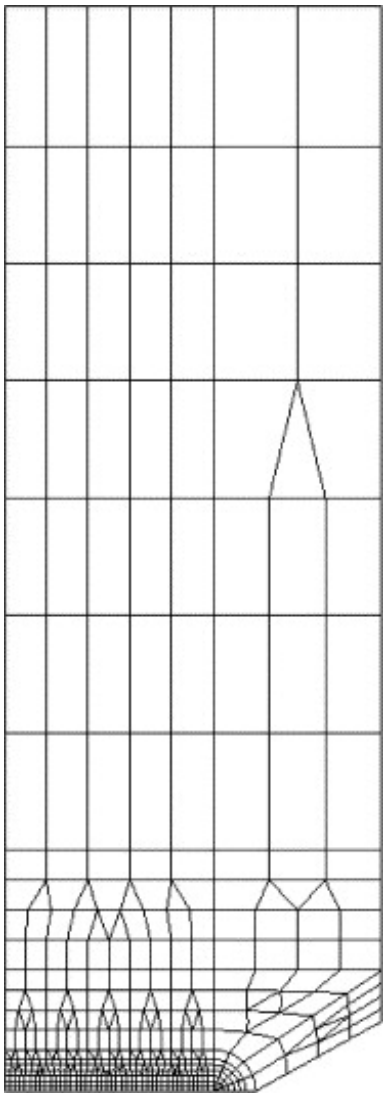

Figure 3: General mesh of the TA30 pre-cracked specimen - Minimum elements 200 microns

Figure 5 compares the load–displacement curve generated by the model with experimental results. This figure demonstrates that the predicted results mirror pretty well the experimental results when the delocalization technique is applied on the $\log$ of the damage parameter. In fact, Enakoutsa *et al.* [4] have demonstrated that applying a simple delocalization technique on the damage parameter results in excessive smoothing of the porosity in the ligament near the crack type, which yields an earlier drop of the load vs. displacement

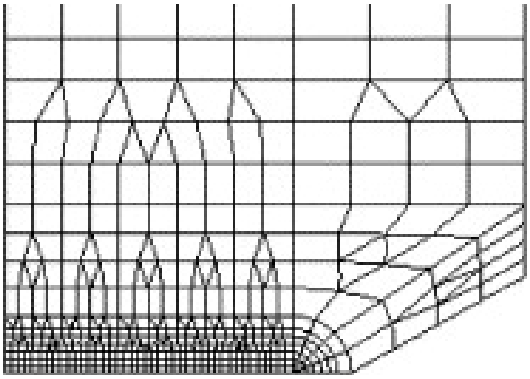

Figure 4: Zoom of the mesh of the TA30 specimen-Minimum element size 200 microns

curve, in contradiction with the experiments.

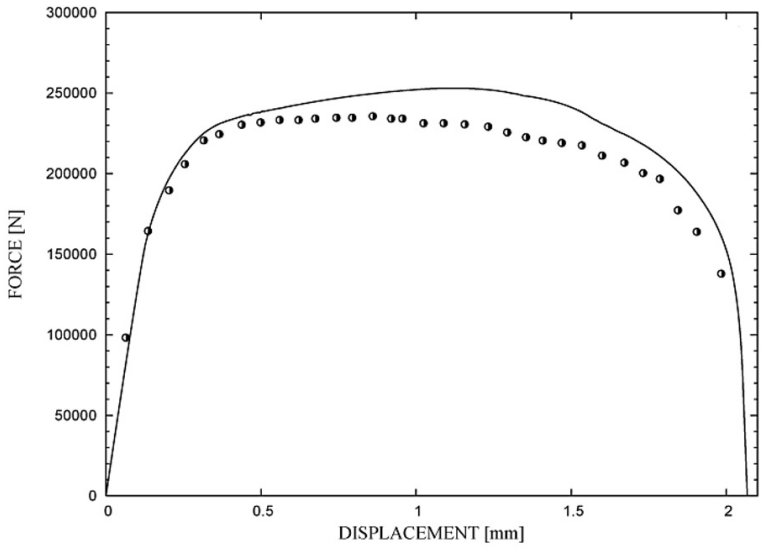

Figure 5: Numerical predictions vs. experiments for the TA30 pre-cracked specimen

6.3. Simulation of a Compact Tension (CT) specimen

In this section, we evaluate the effectiveness of the numerical implementation method in replicating the fracture test conducted by [20]. The test involved a CTJ 25 specimen, made of SS 316L (also called 16MND5 steel) stainless steel, which was deformed under plane strain conditions. The discretized geometry of the specimen is illustrated in Figure 6. To simplify the modeling process, we take advantage of the specimen's symmetry about the vertical mid-plane and only simulate its right half.

The CTJ 25 specimen has dimensions of 50 mm (width), 50 mm (height), and 25 mm (thickness). A rectangular notch with a width of 2mm is located on the top surface. However, as we move towards the notch

root, the shape of the notch transitions into a triangular form, with an opening angle of 60°. It is important to note that a fatigue pre-crack, not visible in the figure, with a length of 1.34 mm originates from the notch root.

In this study, we utilize a single 2D mesh since comprehensive analysis of mesh sensitivity was conducted in the simulations of a TA30 specimen, as described in previous works by the authors [4, 6]

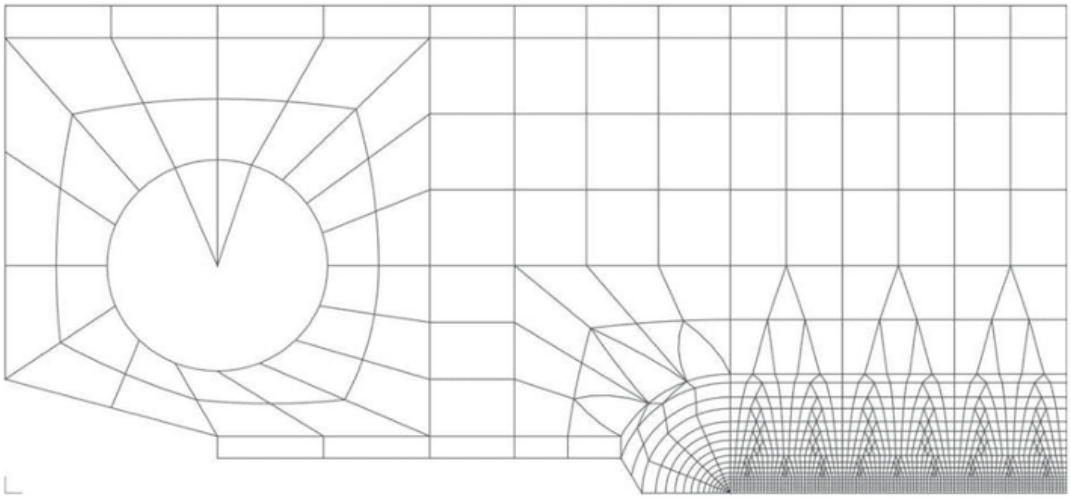

Figure 6: Fine Mesh of the CTJ 25 pre-cracked specimen.

During the experiment, the use of lateral central triangular notches and the opening angle ensured that the region where the crack propagated exhibited nearly plane strain conditions, allowing for a two-dimensional simulation. However, because the assumption of perfect plane strain in such a simulation is not entirely accurate, when comparing the simulation results to the experimental data, it is necessary to adjust the applied experimental force by dividing it by an "equivalent thickness" of the specimen, which slightly deviates from the actual thickness. This matter was extensively investigated by Brosse [3], who determined a "best value" of 10.3 mm for this equivalent thickness, which is adopted in this study. The values of the material parameters are provided in the Table A.1 in the Appendix section.

Figure 7 shows the experimental load–displacement curve (in the black points) together with the numerical ones obtained with the inclusion of the kinematics hardening and isotropic hardening. The simulations show that the results with the inclusion of the kinematics hardening (the results are not shown here) does not change with respect to the isotropic hardening due to the simple tension loading conditions we apply to obtain the numerical results. Also, the results with the numerical simulations with the non-local model (first version) present an excessive smoothing of the porosity in the ligament ahead of the crack tip which leads to am abrupt drop of the load-displacement curve; this can be fixed by using the In of the evolution equation of the porosity (see Figure 7) However, the discrepancy between the numerical predictions generated by the modified non-local Gurson's model (with isotropic hardening) and the actual experimental outcomes is

undeniably significant, demanding an immediate attention. Nevertheless, this disparity can be decisively mitigated through judicious adjustments to the parameters f_c, representing the porosity value at the onset of coalescence, and the cavities growth accelerator factor δ, respectively, leaving no room for compromise.

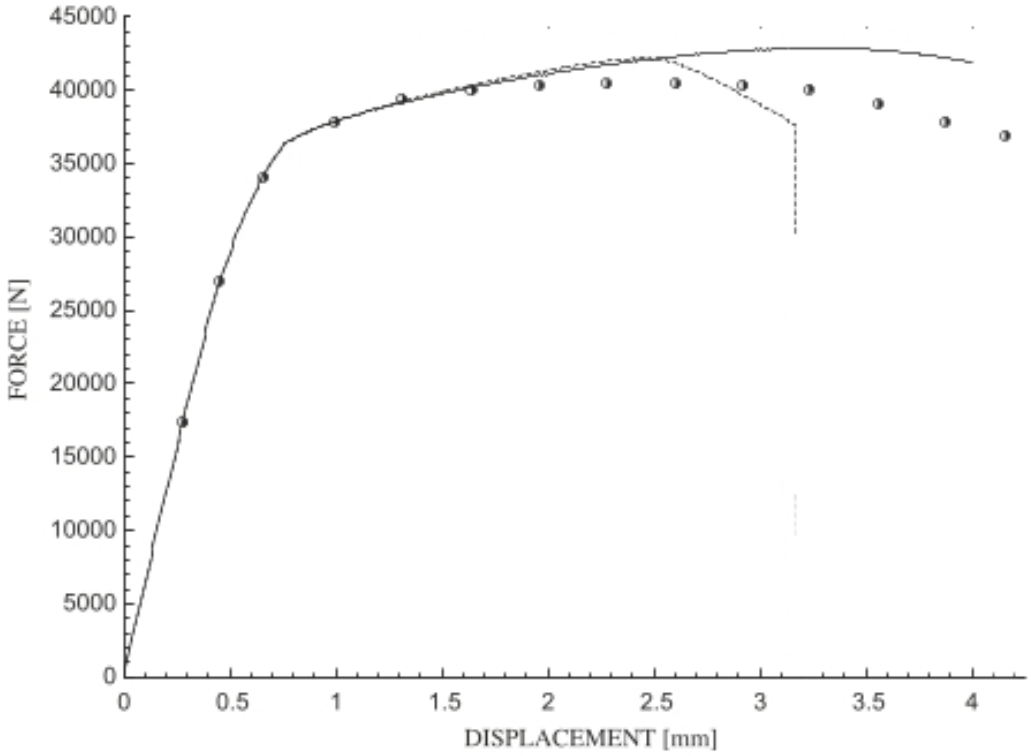

Figure 7: Comparison of experimental and computed load–displacement curves of the CT specimen.

7. Conclusion

The paper presents a comprehensive examination of the numerical implementation and assessment of Perrin's hardening model. The implementation covers three cases: isotropic hardening, kinematic hardening, and mixed isotropic-kinematic hardening. Stiffness matrices of the models are derived to maintain quadratic convergence. Large deformations are accounted for in the implementation, and the model's performance is evaluated by comparing experimental and numerical results in typical ductile fracture tests. The comparison between the experimental and numerical results demonstrates a successful agreement, highlighting the effectiveness of the ductile fracture accounting for hardening model in capturing the behavior of ductile materials

under static loading conditions.

8. Aknowledgments

The authors wish to express their appreciation to the anonymous pre-reviewers for their helpful suggestions which greatly improved the presentation of this paper.

9. Declarations

9.1. Conflict of interest

The authors declare that they have no conflicts of interest to report regarding the present study.

9.2. Funding

The authors did not receive support from any organization for the submitted work.

References

[1] Ahad, F., Enakoutsa, K., Solanki, K., and Bammann, D. (2013). Nonlocal Modeling in High Velocity Impact failure of Aluminum 6160-T6, *Int. J. Plast.,* in Press, doi:10.1016/j.ijplas.2013.10.001.

[2] J. Besson, D. Steglich, W. Brocks, Modeling of crack growth in round bars and plane strain specimens, Int. J. Solids Struct. 38 (2001) 8259–8284.

[3] A. Brosse, Modélisation de déchirure ductile dans un tuyau inox – Calage des paramètres de Wilkins, ESI France Internal, Report F/LE/09/042/D/BPE (in French), 2009.

[4] Enakoutsa K., Leblond J.B. and Perrin G. (2007). Numerical implementation and assessment of a phenomenological nonlocal model of ductile rupture, *Comput. Meth. Appl. Mech. Engng.*, **196**, 1946-1957.

[5] Analytical study of a hollow sphere made of porous plastic material and subjected to hydrostatic tension - Application to some problems in ductile fracture of metals. Int. J. Plast., 6, 677-699.

[6] Enakoutsa K. (2007). Modèle non-locaux en rupture ductile des métaux. Ph.D thesis, Université Pierre et Marie Curie (Paris VI) (in French).

[7] Enakoutsa K., and Leblond J.B. (2009). Numerical implementation and assessment of the GLPD micromorphic model of ductile rupture, *Eur. J. Mech. A/Solids*, **28**, 445-460.

[8] Enakoutsa K. (2012). Some new applications of the GLPD micromorphic model for ductile fracture, *Math. Mech. Solids,* **19**(3), 242-259.

[9] Enakoutsa, K., Solanki, K., Ahad, F., Tjiptowidjojo, Y., and Bammann, D. (2012). Using Damage Delocalization to Model Localization Phenomena in Bammann-Chiesa-Johnson Metals, *J. Eng. Mater. Tech.,* 134(4).

[10] Enakoutsa, K., Solanki, K., Ahad, F., Tjiptowidjojo, Y., and Bammann, D. (2012). Damage smoothing effects in a delocalized rate sensitivity model for metals, *Theoretical and Applied Mechanical Letters,* **2**(5): 5-051005.

[11] J. Devaux, J-B. Leblond, G. Mottet, G. Perrin, Some new applications of damage models for ductile metals, in: Application of Local Fracture/Damage Models to Engineering Problems, Proceedings of the ASME Summer Mechanics Meeting, Tempe (USA), American Society of Mechanical Engineers, 1992.

[12] Gurson A.L. (1977). Continuum theory of ductile rupture by void nucleation and growth: Part I - yield criteria and flow rules for porous ductile media, *ASME J. Engng. Mater. Technol.*, **99**, 2-15.

[13] Perrin, G., 1992. Contribution à l' étude théorique et numérique de la rupture ductile des métaux. Thèse de Doctorat, Ecole Polytechnique, Palaiseau, France.

[14] Pijaudier-Cabot, G., & Bažant, Z. P. (1987). Nonlocal damage theory. Journal of Engineering Mechanics, **113(10)**, 1512-1533.

[15] Leblond, J.B., Perrin, G., and Devaux, J.,1994."Bifurcation Effects in Ductile Metals with Nonlocal Damage", ASME J. Applied . Mech., **61**, 236-242.

[16] Fressengeas, C and Molinari A. (1983). Modèle d'écrouissage cinématique en grande deformation, *C.R.A.S.*, **297 II**, 93.

[17] Fressengeas, C and Molinari A. (1983). Représentation du comportement plastique anisotrope aux grandes deformations, Arch. Mech. **36** , 483.

[18] R. Hill, The essential structure of constitutive laws for metal composites and polycrystals, Journal of the Mechanics and Physics of Solids, Volume **15**, Issue 2, 1967, Pages 79-95.

[19] G. Rousselier, F. Mudry, Etude de la rupture ductile de l'acier faiblement allié en Mn-Ni-Mo pour cuves de réacteurs à eau ordinaire sous pression, approvisionné sous la forme d'une débouchure de tubulure. Résultats du programme expérimental, EdF Centre des Renardières Internal Report HT/PVD529 MAT/T43 (in French), 1980.

[20] J. Devaux, G. Mottet, Etude Numérique de la Rupture Ductile de l'Acier de Cuve 16MND5: Simulation des Eprouvettes Fissurées de Type TA et CTJ, ESI, Report LTSW.92/2036, 1992 (in French).

[21] G. Rousselier, Ductile fracture models and their potential in local approach of fracture, Nuclear Engineering and Design, Volume **105** , Issue 1, 1987, Pages 97-111.

[22] V. Tvergaard, Influence of voids on shear band instabilities under plane strain conditions, Int. J. Fract. 17 (1981) 389–407.

[23] V. Tvergaard, A. Needleman, Analysis of cup-cone fracture in a round tensile bar, Acta Metall. 32 (1984) 157–169.

[24] V. Tvergaard, A. Needleman, Effects of nonlocal damage in porous plastic solids, Int. J. Solids Struct. 32 (1995) 1063–1077.

[25] V. Tvergaard, A. Needleman, Nonlocal effects on localization in a void-sheet, Int. J. Solids Struct. 34 (1997) 2221–2238.

[26] Gologanu M, Leblond JB, Perrin G, Devaux J. Recent extensions of Gurson's model for porous ductile metals. In Suquet P (ed.) Continuum Micromechanics. New York: Springer, 1997, vol. **377**, pp. 61–130.

[27] Mandel J. Contribution theorique a l' etude de l' ecrouissage et des lois d' ecoulement plastique, in: Proceedings of the 11th International Congress on Applied Mechanics, Springer, pp. 502-509 (in French).

Appendix A. Material parameters for the simulations

The material parameters for the simulations presented in above are as follows:

E (Mpa)	ν	Σ_0 (Mpa)	q	f_0	f_c	b	δ
203,000	0.3	450	1.47	0.00016	0.05	0.05	0.2

Table A.1: Material parameters used for the numerical simulations on the TA and the CT specimen

Appendix B. Calculation of the stiffness matrices

Appendix B.1. Generalities

The objective of this section is to expose the calculation of the stiffness matrices for the classical model of ductile damage of Gurson [12], and its alternative due to Leblond-Perrin-Devaux (model LPD) [13] which have improved the modeling of the effects of work hardening in the model which are considered in this work.

Perrin [13] presents the equations of the LPD model and its numerical implementation. Analogous presentation can be found for Gurson's model in Enakoutsa *et al.* [4] and Enakoutsa [6]. With regard to the latter, it will therefore be essential to expose in preliminary the basic equations of the model and its numerical implementation.

The calculation of the stiffness matrix revealed a default of the numerical implementation proposed for the LPD model (and its analogous for the model of Gurson). This default concerns the use, in the flow rule associated with the criterion, of a porosity $f^{\frac{1}{2}}$ at the "half-interval", i.e. at time $t + \frac{\Delta t}{2}$, during the transition from time t to time $t + \Delta t$. The purpose of introducing this porosity was to improve the numerical precision of the algorithm. Unfortunately it presents the serious disadvantage of dissymmetrizing the stiffness matrix in the case of the model of Gurson (one will not seek here to justify this assertion, which would lead us too far). We prefer a slightly different algorithm using, instead of $f'^{\frac{1}{2}}$, the final porosity (at $t + \Delta t$) f. This leads, for Gurson model, to a symmetric matrix. For the LPD model, the matrix obtained will unfortunately be asymmetrical even by taking $f^{\frac{1}{2}} = f$; we will nevertheless favor this choice for the sake of homogeneity with the numerical implementation of Gurson model.

We will not in fact calculate all the terms of the tangent-matrix but only the "most important" ones (or at least that we think so). Thus one will not take into account for the calculation of the stiffness matrix, the variation of the stresses due to the variation of the temperature; this is in fact strictly licit due to the fact that this constraint correction is carried out explicitly, using the constraints at time t and not $t + \Delta t$, and is therefore independent of the displacement increment $\Delta \mathrm{u}$ between these times. We will not take into account either the variation of the stresses due to the objective derivation in the law of hypo-elasticity, which does indeed depend on $\Delta \mathrm{u}$ and therefore theoretically generates a contribution in the tangent-matrix.

Similarly, we will not take into account the influence of the geometry on the residual forces (derivation of $\mathbf{B}$ with respect to $\Delta \mathrm{u}$ in the integral $\int_{\Omega}^{t} \mathbf{B} : \mathbf{\Sigma} \mathrm{dv}$). We can summarize all this by saying that the calculation of the stiffness matrix will be carried out by neglecting the effects of large transformations, that is to say by limiting ourselves to the calculation of $\partial \Sigma_{\mathrm{ij}} \Big/ \partial \Delta \varepsilon_{\mathrm{kl}}$ where Σ denote the stress tensor at $t + \Delta t$ and $\Delta \varepsilon$ the total strain increment (elastic + plastic) between t and $t + \Delta t$. This choice is in conformity with that already made in finite element codes for the computation of the stiffness matrix for the usual models of plasticity (without damage), whose numerical experiments demonstrated the effectiveness.

Appendix B.2. Case of the Gurson model

Appendix B.2.1. New parametrization of the yield criterion and derivation

The quantities Σ_{eq}, Σ_m are expressed as a function of φ and $\bar{\Sigma}$ as follows (see Eq.(85):

$$\begin{cases} \Sigma_{eq} = \bar{\Sigma} S_{eq}, S_{eq} \equiv S_{eq}(\varphi) = (1-p) cos\varphi \\ \\ \Sigma_m = \bar{\Sigma} S_m, S_m \equiv S_m(\varphi) = \frac{2}{3} sgn(\varphi) Argch\left[1 + \frac{(1-p)^2}{2p} sin^2\varphi\right] \end{cases} \tag{B.1}$$

the derivatives of S_{eq} and S_m with respect to φ being given by

$$\begin{cases} \frac{dS_{eq}}{d\varphi} = -(1-p) sin\varphi \\ \\ \frac{dS_m}{d\varphi} = \frac{2}{3} \frac{(1-p)^2}{p} \frac{\sin\varphi cos\varphi}{sh\left(\frac{3}{2} S_m\right)} \end{cases} \tag{B.2}$$

Appendix B.2.2. Derivatives of $\Sigma^{*\prime}, \Sigma^*_m$ and Σ^*_{eq} with respect to $\Delta\varepsilon$

From formulas

$$\Sigma^{*\prime}_{ij} = \Sigma^{o\prime}_{ij} + 2\mu\Delta\varepsilon'_{ij}, \Delta\varepsilon'_{ij} = \Delta\varepsilon_{ij} - \frac{1}{3}\Delta\varepsilon_{kk}\delta_{ij}, \quad \Sigma^*_m = \Sigma^o_m + (3\lambda + 2\mu)\Delta\varepsilon_m = \Sigma^o_m + \frac{1}{3}(3\lambda + 2\mu)\Delta\varepsilon_{kk}, \tag{B.3}$$

we draw immediately:

$$\begin{cases} \frac{\partial\Sigma^{*\prime}_{ij}}{\partial\Delta\varepsilon_{kl}} = 2\mu\left[\frac{1}{2}\left(\delta_{ik}\delta_{jl} + \delta_{il}\delta_{jk}\right) - \frac{1}{3}\delta_{ij}\delta_{kl}\right] \\ \\ \frac{\partial\Sigma^*_m}{\partial\Delta\varepsilon_{kl}} = \frac{1}{3}(3\lambda + 2\mu)\delta_{kl} \end{cases} \tag{B.4}$$

From Eq.(B.4), we deduce that:

$$\frac{\partial\Sigma^*_{eq}}{\partial\Delta\varepsilon_{kl}} = 3\mu\frac{\Sigma^{*\prime}_{kl}}{\Sigma^*_{eq}} \tag{B.5}$$

Appendix B.2.3. Derivatives of $\bar{\Sigma}$ with respect to $\Delta\varepsilon$ and φ

To evaluate these derivatives, we will differentiate the evolution equation Eq.(87) from $\Delta\bar{\varepsilon}$, written in the form:

$$(1-f)\Delta\bar{\varepsilon} = \mathrm{S_{eq}}\Delta\varepsilon^{\mathrm{p}}_{\mathrm{eq}} + 3\mathrm{S_m}\Delta\varepsilon^{\mathrm{p}}_{\mathrm{m}} = \mathrm{S_{eq}}\frac{\Sigma^*_{\mathrm{eq}} - \bar{\Sigma}\mathrm{S_{eq}}}{3\mu} + 3\mathrm{S_m}\frac{\Sigma^*_{\mathrm{m}} - \bar{\Sigma}S_{\mathrm{m}}}{3\lambda+2\mu} \tag{B.6}$$

Before taking this differentiation, note that:

$$\frac{d\mathrm{S_{eq}}}{\mathrm{d}\varphi}\Delta\varepsilon^{\mathrm{p}}_{\mathrm{eq}} + 3\frac{\mathrm{dS_m}}{\mathrm{d}\varphi}\Delta\varepsilon^{\mathrm{p}}_{\mathrm{m}} = 0; \tag{B.7}$$

this property is due to the orthogonality of $\Delta\varepsilon^{\mathrm{p}}$ to the yield surface ($\boldsymbol{\Sigma} : \Delta\varepsilon^{\mathrm{p}} = \mathrm{d}\Sigma_{\mathrm{eq}}\Delta\varepsilon^{\mathrm{p}}_{\mathrm{eq}} + 3\mathrm{d}\Sigma_{\mathrm{m}}\Delta\mathrm{c}^{\mathrm{p}}_{\mathrm{m}} = 0$ if we vary Σ on the yield surface, i.e. if we vary φ, at $\bar{\Sigma}$ fixed). Given this remark, the differentiation gives:

$$\begin{aligned}(1-f)\mathrm{d}\Delta\bar{\varepsilon} = &\left(\frac{\mathrm{S_{eq}}}{3\mu}\frac{\partial\Sigma^*_{\mathrm{eq}}}{\partial\Delta\mathrm{e_{kj}}} + \frac{3\mathrm{S_m}}{3\lambda+2\mu}\frac{\partial\Sigma^*_{\mathrm{m}}}{\partial\Delta\varepsilon_{\mathrm{kl}}}\right)\mathrm{d}\Delta\varepsilon_{\mathrm{kl}}\\ &-\left(\frac{\Sigma_{\mathrm{eq}}}{3\mu}\frac{\mathrm{dS_{eq}}}{\mathrm{d}\phi} + \frac{3\Sigma_{\mathrm{m}}}{3\lambda+2\mu}\frac{\mathrm{dS_m}}{\mathrm{d}\phi}\right)\mathrm{d}\phi - \left(\frac{\mathrm{S^2_{eq}}}{3\mu} + \frac{3\mathrm{S^2_m}}{3\lambda+2\mu}\right)\frac{\mathrm{d}\bar{\Sigma}}{\mathrm{d}\bar{\varepsilon}}\mathrm{d}\Delta\bar{\varepsilon}\end{aligned} \tag{B.8}$$

At $\varphi = const$, this gives:

$$\frac{\partial\bar{\varepsilon}}{\partial\Delta\varepsilon_{\mathrm{kj}}} = \frac{\frac{\mathrm{S_{eq}}}{3\mu}\frac{\partial\Sigma^*_{\mathrm{eq}}}{\partial\Delta\mathrm{c_{kj}}} + \frac{3\mathrm{S_m}}{3\lambda+2\mu}\frac{\partial\Sigma^*_{\mathrm{m}}}{\partial\Delta\mathrm{r_{kl}}}}{(1-f) + \left(\frac{\mathrm{S^2_{eq}}}{3\mu} + \frac{3\mathrm{S^2_m}}{3\lambda+2\mu}\right)\frac{\mathrm{d}\bar{\Sigma}}{\mathrm{de}}} \quad \left(\text{and} \quad \frac{\partial\bar{\Sigma}}{\partial\Delta\varepsilon_{\mathrm{kl}}} = \frac{\mathrm{d}\bar{\Sigma}}{\mathrm{d}\bar{\varepsilon}}\frac{\partial\Delta\bar{\varepsilon}}{\partial\Delta\varepsilon_{\mathrm{kl}}}\right); \tag{B.9}$$

at $\Delta\varepsilon = const$, we get:

$$\frac{\partial\Delta\bar{\varepsilon}}{\partial\varphi} = -\frac{\frac{\Sigma_{\mathrm{eq}}}{3\mu}\frac{\mathrm{dS_{eq}}}{\mathrm{d}\varphi} + \frac{3\Sigma_{\mathrm{m}}}{3\lambda+2\mu}\frac{\mathrm{dS_m}}{\mathrm{d}\varphi}}{(1-f) + \left(\frac{\mathrm{S^2_{eq}}}{3\mu} + \frac{3\mathrm{S^2_m}}{3\lambda+2\mu}\right)\frac{\mathrm{d}\bar{\Sigma}}{\mathrm{d}\bar{\varepsilon}}} \quad \left(\text{and} \quad \frac{\partial\bar{\Sigma}}{\partial\varphi} = \frac{\mathrm{d}\bar{\Sigma}}{\mathrm{d}\bar{\varepsilon}}\frac{\partial\bar{\varepsilon}}{\partial\varphi}\right) \tag{B.10}$$

Appendix B.2.4. Derivatives of φ with respect to $\Delta\varepsilon$

It is now necessary to exploit the fundamental equation Eq.(90) giving φ. Note that the stresses $\Sigma_{\mathrm{eq}^*}, \Sigma^*_{\mathrm{m}}$ depend only on $\Delta\varepsilon$, while the constraints $\sigma_{\mathrm{eq}}, \Sigma_{\mathrm{m}}$ depend on φ and $\bar{\Sigma}$. So this equation is written as:

$$\mathrm{F}(\Delta\varepsilon, \varphi, \bar{\Sigma}) = a\left[\Sigma^*_{\mathrm{m}}(\Delta\varepsilon) - \bar{\Sigma}\mathrm{S_m}(\varphi)\right]cos\varphi - p\left[\Sigma^*_{\mathrm{eq}}(\Delta\varepsilon) - \bar{\Sigma}\mathrm{S_{eq}}(\varphi)\right]sh\left[\frac{3}{2}\mathrm{S_m}(\varphi)\right] = 0 \tag{B.11}$$

By differentiating, we get

$$\frac{\partial \mathrm{F}}{\partial \Delta\varepsilon_{\mathrm{kl}}}\mathrm{d}\Delta\varepsilon_{\mathrm{kl}} + \frac{\partial \mathrm{F}}{\partial \varphi}\mathrm{d}\varphi + \frac{\partial \mathrm{F}}{\partial \bar{\Sigma}}\mathrm{d}\bar{\Sigma} = 0. \tag{B.12}$$

where

$$\frac{\partial \mathrm{F}}{\partial \Delta\varepsilon_{\mathrm{kl}}} = \frac{\partial \mathrm{F}}{\partial \Sigma^*_{\mathrm{eq}}}\frac{\partial \Sigma^*_{\mathrm{eq}}}{\partial \Delta\varepsilon_{\mathrm{kl}}} + \frac{\partial \mathrm{F}}{\partial \Sigma^*_{m}}\frac{\partial \Sigma^*_{\mathrm{m}}}{\partial \Delta\varepsilon_{\mathrm{kl}}}, \quad \frac{\partial \mathrm{F}}{\partial \Sigma^*_{\mathrm{eq}}} = -p\, sh\left(\frac{3}{2}\mathrm{S_m}\right), \quad \frac{\partial \mathrm{F}}{\partial \Sigma^*_{\mathrm{m}}} = a cos\varphi, \tag{B.13}$$

$$\frac{\partial \mathrm{F}}{\partial \varphi} = p\bar{\Sigma} sh\left(\frac{3}{2}\mathrm{S_m}\right)\frac{\mathrm{dS_{eq}}}{\mathrm{d}\varphi} - \left[a\bar{\Sigma} cos\varphi + \frac{3}{2}p\left(\Sigma^*_{\mathrm{eq}} - \Sigma_{\mathrm{eq}}\right)\mathrm{ch}\left(\frac{3}{2}\mathrm{S_m}\right)\right]\frac{d\mathrm{S_m}}{\mathrm{d}\varphi} - a\left(\Sigma^*_{\mathrm{m}} - \Sigma_{\mathrm{m}}\right) sin\varphi \tag{B.14}$$

$$\frac{\partial \mathrm{F}}{\partial \bar{\Sigma}} = -a\mathrm{S_m} cos\varphi + p\mathrm{S_{eq}} sh\left(\frac{3}{2}\mathrm{S_m}\right) \tag{B.15}$$

By expanding $d\bar{\Sigma} = \dfrac{\partial \bar{\Sigma}}{\partial \Delta\varepsilon_{\mathrm{kl}}}\mathrm{d}\Delta\varepsilon_{\mathrm{k}} + \dfrac{\partial \bar{\Sigma}}{\partial \varphi}\mathrm{d}\varphi$ in Eq.(B.12), we get:

$$\frac{\partial \mathrm{F}}{\partial \Delta\varepsilon_{\mathrm{kl}}}\mathrm{d}\Delta\varepsilon_{\mathrm{kl}} + \frac{\partial \mathrm{F}}{\partial \varphi}\mathrm{d}\varphi + \frac{\partial \mathrm{F}}{\partial \Sigma}\frac{\partial \Sigma}{\partial \Delta\varepsilon_{\mathrm{kl}}}\mathrm{d}\Delta\varepsilon_{\mathrm{k}} + \frac{\partial \mathrm{F}}{\partial \Sigma}\frac{\partial \sigma}{\partial \varphi}\mathrm{d}\varphi = 0 \tag{B.16}$$

and thus

$$\frac{\partial \varphi}{\partial \Delta\varepsilon_{\mathrm{kl}}} = -\frac{\dfrac{\partial \mathrm{F}}{\partial \Delta\varepsilon_{\mathrm{kl}}} + \dfrac{\partial \mathrm{F}}{\partial \bar{\Sigma}}\dfrac{\partial \bar{\Sigma}}{\partial \Delta\varepsilon_{\mathrm{kl}}}}{\dfrac{\partial \mathrm{F}}{\partial \varphi} + \dfrac{\partial \mathrm{F}}{\partial \bar{\Sigma}}\dfrac{\partial \bar{\Sigma}}{\partial \varphi}}. \tag{B.17}$$

Note that the derivative $\partial F \Big/ \partial \varphi$ is precisely the "slope" which intervenes in Newton's method on φ used to solve equation Eq.(B.16).

Appendix B.2.5. Derivatives of Σ_{eq} *and* Σ_{m} *with respect to* $\Delta\varepsilon$

We have $\Sigma_{\mathrm{eq}} = \bar{\Sigma}_{\mathrm{eq}}, \bar{\Sigma}$ depending on $\Delta\varepsilon$ and φ, and $\mathrm{S_{eq}}$ of φ alone, φ being itself a function of $\Delta\varepsilon$. Therefore:

$$\frac{\partial \Sigma_{\mathrm{eq}}}{\partial \Delta\varepsilon_{\mathrm{kl}}} = \mathrm{S_{eq}}\frac{\partial \bar{\Sigma}}{\partial \Delta\varepsilon_{\mathrm{kl}}} + \mathrm{S_{eq}}\frac{\partial \bar{\Sigma}}{\partial \varphi}\frac{\partial \varphi}{\partial \Delta\varepsilon_{\mathrm{kl}}} + \bar{\Sigma}\frac{d\mathrm{S_{eq}}}{d\varphi}\frac{\partial \varphi}{\partial \Delta\varepsilon_{\mathrm{kl}}} \tag{B.18}$$

Also,

$$\frac{\partial \Sigma_{\mathrm{m}}}{\partial \Delta \varepsilon_{\mathrm{kl}}} = \mathrm{S}_{\mathrm{m}} \frac{\partial \bar{\Sigma}}{\partial \Delta \varepsilon_{\mathrm{kl}}} + \mathrm{S}_{\mathrm{m}} \frac{\partial \bar{\Sigma}}{\partial \varphi} \frac{\partial \varphi}{\partial \Delta \varepsilon_{\mathrm{kl}}} + \bar{\Sigma} \frac{\mathrm{S}_{\mathrm{m}}}{\mathrm{d}\varphi} \frac{\partial \varphi}{\partial \Delta \varepsilon_{\mathrm{kl}}} \tag{B.19}$$

Appendix B.2.6. Derivatives of Σ' and Σ with respect to $\Delta\varepsilon$

The differentiation of the equation $\dot{\Sigma}'_{\mathrm{ij}} = \frac{\Sigma_{\mathrm{eq}}}{\Sigma^*_{\mathrm{eq}}} \Sigma^{*\prime}_{\mathrm{ij}}$ gives

$$\frac{\partial \Sigma^*_{\mathrm{ij}}}{\partial \Delta \varepsilon_{\mathrm{kl}}} = \frac{\Sigma_{\mathrm{eq}}}{\Sigma^*_{\mathrm{eq}}} \frac{\partial \Sigma^*_{\mathrm{ij}}}{\partial \Delta \varepsilon_{\mathrm{kl}}} + \Sigma^*_{\mathrm{ij}} \left(\frac{1}{\Sigma^*_{\mathrm{eq}}} \frac{\partial \Sigma_{\mathrm{eq}}}{\partial \Delta \varepsilon_{\mathrm{k}}} - \frac{\Sigma_{\mathrm{eq}}}{\Sigma^{*2}_{\mathrm{eq}}} \frac{\partial \Sigma^*_{\mathrm{eq}}}{\partial \Delta \varepsilon_{\mathrm{kl}}} \right) \tag{B.20}$$

Finally, the equation $\Sigma_{\mathrm{ij}} = \Sigma'_{\mathrm{ij}} + \Sigma_{\mathrm{m}} \delta_{\mathrm{ij}}$ gives

$$\frac{\partial \Sigma_{\mathrm{ij}}}{\partial \Delta \varepsilon_{\mathrm{kl}}} = \frac{\partial \Sigma'_{\mathrm{ij}}}{\partial \Delta \varepsilon_{\mathrm{kl}}} + \frac{\partial \Sigma_{\mathrm{m}}}{\partial \Delta \varepsilon_{\mathrm{kl}}} \delta_{\mathrm{ij}} \tag{B.21}$$

This completes the calculation of the tangent-matrix for the Gurson model [12].

Appendix B.3. Case of the LPD model

Appendix B.3.1. Yield locus parametrization

The stress $\Sigma_{\rm eq}, \Sigma_{\rm m}$ are expressed here as a function of φ, σ_1 and Σ_2 as follows:

$$\begin{cases} \Sigma_{eq} = \Sigma_1 \mathrm{S}_{\rm eq}(\varphi) \\ \Sigma_{\rm m} = \Sigma_2 \mathrm{S}_{\rm m}(\varphi) \end{cases} \tag{B.22}$$

where the expressions for $\mathrm{S}_{\rm eq}(\varphi)$ and $S_{\rm m}(\varphi)$, as well as their derivatives, are the same as for the Gurson model (Eq.(B.1) and Eq.(B.2))

Appendix B.3.2. Differentials of $\varepsilon_{\rm eq}$ and $\Sigma_{\rm m}$

From the equation of evolution of the hardening parameter ε_{eq}, i.e. $\dot{\varepsilon}_{\rm eq} = \dot{\varepsilon}^{\rm p}_{\rm eq}$, we deduce that

$$\varepsilon_{\rm eq} = \varepsilon^{\rm o}_{\rm eq} + \Delta\varepsilon^{\rm p}_{\rm eq} \tag{B.23}$$

$$\Rightarrow \mathrm{d}\varepsilon_{\rm eq} = \mathrm{d}\Delta\varepsilon^{\rm p}_{\rm eq} \tag{B.24}$$

Similarly, from the evolution equation $\dot{\varepsilon}_{\rm m} = |\dot{\varepsilon}_{\rm m}|$, we deduce that:

$$\varepsilon_{\rm m} = \varepsilon^{*}_{\rm m} + \left|\Delta\varepsilon^{\rm p}_{\rm m}\right| \tag{B.25}$$

$$\Rightarrow \mathrm{d}\varepsilon_{\rm m} = sgn\left(\Delta\varepsilon^{\rm p}_{\rm m}\right)\mathrm{d}\Delta\varepsilon^{\rm p}_{\rm m} \tag{B.26}$$

The sign of $\Delta\varepsilon^{\rm p}_{\rm m}$ is the same as that of Σ_m, that is to say of φ according to Eq.(B.22)$_2$ and the expression of $\mathrm{S}_{\rm m}(\varphi)$ (cf. Eq.(B.1)). Therefore

$$\mathrm{d}\varepsilon_{\rm m} = \varepsilon\,\mathrm{d}\Delta\varepsilon^{\rm p}_{\rm m}, \quad \varepsilon = sgn(\varphi) \tag{B.27}$$

Appendix B.3.3. Derivatives of Σ_1 and Σ_2 with respect to $\Delta\varepsilon$ and φ

Let us recall that Σ_1 and Σ_2 are known, pre-tabulated functions of the hardening parameters $\varepsilon_{\rm eq}, \varepsilon_m$ (and of the initial porosity). We have:

$$d\Sigma_1 = \frac{\partial\Sigma_1}{\partial\varepsilon_{\rm eq}}\mathrm{d}\varepsilon_{\rm eq} + \frac{\partial\Sigma_1}{\partial\varepsilon_{\rm m}}\mathrm{d}\varepsilon_{\rm m} = \frac{\partial\Sigma_1}{\partial\varepsilon_{\rm eq}}\mathrm{d}\Delta\varepsilon_{\rm eq} + \frac{\partial\Sigma_1}{\partial\varepsilon_{\rm m}}\varepsilon\mathrm{d}\Delta\varepsilon^{\rm p}_{\rm m} \tag{B.28}$$

from Eq.(B.24) and Eq.(B.27). Now,

$$\Delta\varepsilon^{\rm p}_{eq} = \frac{\Sigma^{*}_{\rm eq} - \Sigma_{\rm eq}}{3\mu} = \frac{1}{3\mu}\left(\Sigma^{*}_{\rm eq} - \Sigma_1\mathrm{S}_{\rm eq}\right) \tag{B.29}$$

$$\Rightarrow \mathrm{d}\Delta\varepsilon_{\mathrm{eq}}^{\mathrm{p}} = \frac{1}{3\mu}\left(\frac{\partial\Sigma_{\mathrm{eq}}^{*}}{\partial\Delta\varepsilon_{\mathrm{kl}}}\mathrm{d}\Delta\varepsilon_{\mathrm{kd}} - \Sigma_{1}\frac{\mathrm{dS_{eq}}}{\mathrm{d}\varphi}\mathrm{d}\varphi - \mathrm{S_{eq}}\mathrm{d}\Sigma_{1}\right) \tag{B.30}$$

Also,

$$\Delta\varepsilon_{\mathrm{m}}^{\mathrm{p}} = \frac{1}{3\lambda + 2\mu}\left(\Sigma_{\mathrm{m}}^{*} - \Sigma_{2}\mathrm{S_{m}}\right) \tag{B.31}$$

$$\Rightarrow \mathrm{d}\Delta\varepsilon_{\mathrm{m}}^{\mathrm{p}} = \frac{1}{3\lambda + 2\mu}\left(\frac{\partial\Sigma_{\mathrm{m}}^{*}}{\partial\Delta\varepsilon_{\mathrm{kl}}}\mathrm{d}\Delta\varepsilon_{\mathrm{kl}} - \Sigma_{2}\frac{\mathrm{dS_{m}}}{\mathrm{d}\varphi}\mathrm{d}\varphi - \mathrm{S_{m}}\mathrm{d}\sigma_{2}\right) \tag{B.32}$$

It goes without saying that the expressions of $\partial\Sigma_{\mathrm{eq}}^{*}\Big/\partial\Delta\varepsilon_{\mathrm{kl}}$ and $\partial\Sigma_{\mathrm{m}}^{*}\Big/\mathrm{d}\Delta\varepsilon_{\mathrm{kJ}}$ here are the same as for Gurson model (equations Eq.(B.4), Eq.(B.5)). By transferring these expressions into Eq.(B.28), we obtain:

$$\begin{aligned}\mathrm{d}\Sigma_{1} = {} & \frac{1}{3\mu}\frac{\partial\Sigma_{1}}{\partial\varepsilon_{\mathrm{eq}}}\left(\frac{\partial\Sigma_{\mathrm{eq}}^{*}}{\partial\Delta\varepsilon_{\mathrm{kl}}}\mathrm{d}\Delta\varepsilon_{\mathrm{kl}} - \Sigma_{1}\frac{\mathrm{dS_{eq}}}{\mathrm{d}\varphi}\mathrm{d}\varphi - \mathrm{S_{eq}}\mathrm{d}\Sigma_{1}\right) \\ & + \frac{\varepsilon}{3\lambda + 2\mu}\frac{\partial\Sigma_{1}}{\partial\varepsilon_{\mathrm{m}}}\left(\frac{\partial\Sigma_{\mathrm{m}}^{*}}{\partial\Delta\varepsilon_{\mathrm{kl}}}\mathrm{d}\Delta\varepsilon_{\mathrm{kl}} - \Sigma_{2}\frac{\mathrm{dS_{m}}}{\mathrm{d}\varphi}\mathrm{d}\varphi - \mathrm{S_{m}}\mathrm{d}\Sigma_{2}\right)\end{aligned} \tag{B.33}$$

By reasoning in the same way for Σ_2, we obtain:

$$\begin{aligned}\mathrm{d}\Sigma_{2} = {} & \frac{1}{3\mu}\frac{\partial\Sigma_{2}}{\partial\varepsilon_{\mathrm{eq}}}\left(\frac{\partial\Sigma_{\mathrm{eq}}^{*}}{\partial\Delta\varepsilon_{\mathrm{kl}}}\mathrm{d}\Delta\varepsilon_{\mathrm{kl}} - \Sigma_{1}\frac{\mathrm{dS_{eq}}}{\mathrm{d}\varphi}\mathrm{d}\varphi - \mathrm{S_{eq}}\mathrm{d}\Sigma_{1}\right) \\ & + \frac{\varepsilon}{3\lambda + 2\mu}\frac{\partial\Sigma_{2}}{\partial\varepsilon_{\mathrm{m}}}\left(\frac{\partial\Sigma_{\mathrm{m}}^{*}}{\partial\Delta\varepsilon_{\mathrm{kl}}}\mathrm{d}\Delta\varepsilon_{\mathrm{kl}} - \Sigma_{2}\frac{\mathrm{dS_{m}}}{\mathrm{d}\varphi}\mathrm{d}\varphi - \mathrm{S_{m}}\mathrm{d}\Sigma_{2}\right)\end{aligned} \tag{B.34}$$

By successively taking $\varphi = const$ then $\Delta\varepsilon = const$ in these equations, we obtain the following two systems:

$$\begin{cases} \left(1 + \dfrac{\mathrm{S_{eq}}}{3\mu}\dfrac{\partial\Sigma_{1}}{\partial\varepsilon_{\mathrm{eq}}}\right)\dfrac{\partial\Sigma_{1}}{\partial\Delta\varepsilon_{\mathrm{kl}}} + \dfrac{\varepsilon S_{\mathrm{m}}}{3\lambda + 2\mu}\dfrac{\partial\Sigma_{1}}{\partial\varepsilon_{\mathrm{m}}}\dfrac{\partial\Sigma_{2}}{\partial\Delta\varepsilon_{\mathrm{kl}}} = \dfrac{1}{3\mu}\dfrac{\partial\Sigma_{1}}{\partial\varepsilon_{\mathrm{eq}}}\dfrac{\partial\Sigma_{\mathrm{eq}}^{*}}{\partial\Delta\varepsilon_{\mathrm{kl}}} + \dfrac{\varepsilon}{3\lambda + 2\mu}\dfrac{\partial\Sigma_{1}}{\partial\varepsilon_{\mathrm{m}}}\dfrac{\partial\Sigma_{\mathrm{m}}^{*}}{\partial\Delta\varepsilon_{\mathrm{kl}}} \\ \dfrac{\mathrm{S_{eq}}}{3\mu}\dfrac{\partial\Sigma_{2}}{\partial\varepsilon_{\mathrm{eq}}}\dfrac{\partial\Sigma_{1}}{\partial\Delta\varepsilon_{\mathrm{kl}}} + \left(1 + \dfrac{\varepsilon S_{\mathrm{m}}}{3\lambda + 2\mu}\dfrac{\partial\Sigma_{2}}{\partial\varepsilon_{\mathrm{m}}}\right)\dfrac{\partial\Sigma_{2}}{\partial\Delta\varepsilon_{\mathrm{kl}}} = \dfrac{1}{3\mu}\dfrac{\partial\Sigma_{2}}{\partial\varepsilon_{\mathrm{eq}}}\dfrac{\partial\Sigma_{\mathrm{eq}}^{*}}{\partial\Delta\varepsilon_{\mathrm{kl}}} + \dfrac{\varepsilon}{3\lambda + 2\mu}\dfrac{\partial\Sigma_{2}}{\partial\varepsilon_{\mathrm{m}}}\dfrac{\partial\Sigma_{\mathrm{m}}^{*}}{\partial\Delta\varepsilon_{\mathrm{kl}}} \end{cases} \tag{B.35}$$

$$\begin{cases} \left(1+\dfrac{\mathrm{S_{eq}}}{3\mu}\dfrac{\partial\Sigma_1}{\partial\varepsilon_{\mathrm{eq}}}\right)\dfrac{\partial\Sigma_1}{\partial\varphi}+\dfrac{\varepsilon S_{\mathrm{m}}}{3\lambda+2\mu}\dfrac{\partial\Sigma_1}{\partial\varepsilon_{\mathrm{m}}}\dfrac{\partial\Sigma_2}{\partial\varphi}=-\dfrac{\Sigma_1}{3\mu}\dfrac{\partial\Sigma_1}{\partial\varepsilon_{\mathrm{eq}}}\dfrac{\mathrm{dS_{eq}}}{\mathrm{d}\varphi}-\dfrac{\varepsilon\Sigma_2}{3\lambda+2\mu}\dfrac{\partial\Sigma_1}{\partial\varepsilon_{\mathrm{m}}}\dfrac{\partial\mathrm{S_m}}{\partial\varphi} \\ \dfrac{\mathrm{S_{eq}}}{3\mu}\dfrac{\partial\Sigma_2}{\partial\varepsilon_{\mathrm{eq}}}\dfrac{\partial\Sigma_1}{\partial\varphi}+\left(1+\dfrac{\varepsilon\mathrm{S_m}}{3\lambda+2\mu}\dfrac{\partial\Sigma_2}{\partial\varepsilon_{\mathrm{m}}}\right)\dfrac{\partial\Sigma_2}{\partial\varphi}=-\dfrac{\Sigma_1}{3\mu}\dfrac{\partial\Sigma_2}{\partial\varepsilon_{\mathrm{eq}}}\dfrac{\mathrm{dS_{eq}}}{\mathrm{d}\varphi}-\dfrac{\varepsilon\Sigma_2}{3\lambda+2\mu}\dfrac{\partial\Sigma_2}{\partial\varepsilon_{\mathrm{m}}}\dfrac{\mathrm{dS_m}}{\partial\varphi}. \end{cases} \tag{B.36}$$

Solving these systems provides the value of the derivatives $\partial\Sigma_1\Big/\mathrm{d}\Delta\varepsilon_{\mathrm{kl}}, \partial\Sigma_2\Big/\mathrm{d}\Delta\varepsilon_{\mathrm{kl}}$, $\partial\Sigma_1\Big/\partial\varphi, \partial\Sigma_2\Big/\partial\varphi$. Note that the matrix 2×2 appearing in the first member is the same for the two systems.

Appendix B.3.4. Derivative of φ with respect to $\Delta\varepsilon$

The fundamental equation giving φ is written:

$$\mathrm{F}\left(\Delta\varepsilon,\varphi,\Sigma_1,\Sigma_2\right)=\mathrm{a}\frac{\Sigma_2}{\Sigma_1}\left[\Sigma^*_{\mathrm{m}}(\Delta\varepsilon)-\Sigma_2\mathrm{S_m}(\varphi)\right]cos\varphi-p\left[\Sigma^*_{\mathrm{eq}}(\Delta\varepsilon)-\Sigma_1\mathrm{S_{eq}}(\varphi)\right]sh\left[\frac{3}{2}\mathrm{S_m}(\varphi)\right]=0 \tag{B.37}$$

Its differentiation gives

$$\frac{\partial\mathrm{F}}{\partial\Delta\varepsilon_{\mathrm{kl}}}\mathrm{d}\Delta\varepsilon_{\mathrm{kl}}+\frac{\partial\mathrm{F}}{\partial\phi}\mathrm{d}\varphi+\frac{\partial\mathrm{F}}{\partial\Sigma_1}\mathrm{d}\Sigma_1+\frac{\partial\mathrm{F}}{\partial\Sigma_2}\mathrm{d}\Sigma_2=0 \tag{B.38}$$

where

$$\frac{\partial\mathrm{F}}{\partial\Delta\varepsilon_{\mathrm{kl}}}=\frac{\partial\mathrm{F}}{\partial\Sigma^*_{\mathrm{eq}}}\frac{\partial\Sigma^*_{\mathrm{eq}}}{\partial\Delta\varepsilon_{\mathrm{kl}}}+\frac{\partial\mathrm{F}}{\partial\Sigma^*_{\mathrm{m}}}\frac{\partial\Sigma^*_{\mathrm{m}}}{\partial\Delta\varepsilon_{\mathrm{kl}}},\ \frac{\partial\mathrm{F}}{\partial\Sigma^*_{\mathrm{eq}}}=-psh\left(\frac{3}{2}S_{\mathrm{m}}\right),\ \frac{\partial\mathrm{F}}{\partial\Sigma^*_{\mathrm{m}}}=a\frac{\Sigma_2}{\Sigma_1}cos\varphi, \tag{B.39}$$

$$\frac{\partial\mathrm{F}}{\partial\varphi}=p\Sigma_1 sh\left(\frac{3}{2}\mathrm{S_m}\right)\frac{\mathrm{dS_{eq}}}{\mathrm{d}\varphi}-\left[a\frac{\Sigma_2^2}{\Sigma_1}cos\varphi+\frac{3}{2}p\left(\Sigma^*_{\mathrm{eq}}-\Sigma_{\mathrm{eq}}\right)ch\left(\frac{3}{2}\mathrm{S_m}\right)\right]\frac{\mathrm{dS_m}}{\mathrm{d}\varphi}-a\frac{\Sigma_2}{\Sigma_1}\left(\Sigma^*_{\mathrm{m}}-\Sigma_{\mathrm{m}}\right)sin\varphi, \tag{B.40}$$

$$\frac{\partial\mathrm{F}}{\partial\Sigma_1}=-a\frac{\Sigma_2}{\Sigma_1^2}\left(\Sigma^*_{\mathrm{m}}-\Sigma_{\mathrm{m}}\right)cos\varphi+p\mathrm{S_{eq}}\ sh\left(\frac{3}{2}S_{\mathrm{m}}\right),\ \frac{\partial\mathrm{F}}{\partial\Sigma_2}=\frac{a}{\Sigma_1}\left(\Sigma^*_{\mathrm{m}}-2\Sigma_{\mathrm{m}}\right)cos\varphi \tag{B.41}$$

By expanding $\mathrm{d}\Sigma_1=\dfrac{\partial\Sigma_1}{\partial\Delta\varepsilon_{\mathrm{kl}}}\mathrm{d}\Delta\varepsilon_{\mathrm{kl}}+\dfrac{\partial\Sigma_1}{\partial\varphi}\mathrm{d}\varphi$ and $\mathrm{d}\Sigma_2=\dfrac{\partial\Sigma_2}{\partial\Delta\varepsilon_{\mathrm{kl}}}\mathrm{d}\Delta\varepsilon_{\mathrm{kl}}+\dfrac{\partial\Sigma_2}{\partial\varphi}\mathrm{d}\varphi$ in Eq.(B.38), we obtain:

$$\frac{\partial\mathrm{F}}{\partial\Delta\varepsilon_{\mathrm{kl}}}\mathrm{d}\Delta\varepsilon_{\mathrm{kl}}+\frac{\partial\mathrm{F}}{\partial\varphi}\mathrm{d}\varphi+\frac{\partial\mathrm{F}}{\partial\Sigma_1}\frac{\partial\Sigma_1}{\partial\Delta\varepsilon_{\mathrm{kl}}}\mathrm{d}\Delta\varepsilon_{\mathrm{kl}}+\frac{\partial\mathrm{F}}{\partial\Sigma_1}\frac{\partial\Sigma_1}{\partial\varphi}\mathrm{d}\varphi+\frac{\partial\mathrm{F}}{\partial\Sigma_2}\frac{\partial\Sigma_2}{\partial\Delta\varepsilon_{\mathrm{kl}}}\mathrm{d}\Delta\varepsilon_{\mathrm{kl}}+\frac{\partial\mathrm{F}}{\partial\Sigma_2}\frac{\partial\Sigma_2}{\partial\varphi}\mathrm{d}\varphi=0 \tag{B.42}$$

and thus

$$\frac{\partial \varphi}{\partial \Delta \varepsilon_{kl}} = -\frac{\dfrac{\partial F}{\partial \Delta \varepsilon_{kl}} + \dfrac{\partial F}{\partial \Sigma_1}\dfrac{\partial \Sigma_1}{\partial \Delta \varepsilon_{kl}} + \dfrac{\partial F}{\partial \Sigma_2}\dfrac{\partial \Sigma_2}{\partial \Delta \varepsilon_{kl}}}{\dfrac{\partial F}{\partial \varphi} + \dfrac{\partial F}{\partial \Sigma_1}\dfrac{\partial \Sigma_1}{\partial \varphi} + \dfrac{\partial F}{\partial \Sigma_2}\dfrac{\partial \Sigma_2}{\partial \varphi}}. \tag{B.43}$$

Here again, we notice that $\partial F \Big/ \partial \varphi$ is the ”slope” used in Newton’s method to solve Eq.(32).